

**ASTROCYTIC MODULATION OF EXCITATORY NEURONAL SIGNALING IN A
MOUSE MODEL OF RETT SYNDROME**

By

Benjamin Rakela

A THESIS

School of Medicine
Oregon Health and Science University

We, the dissertation committee, hereby certify that the Ph.D. dissertation of

Benjamin Rakela

has been approved

Paul Brehm, Ph.D., Senior Scientist, Dissertation Co-Advisor
Vollum Institute for Advanced Biomedical Research

Gail Mandel, Ph.D., Senior Scientist, Dissertation Co-Advisor
Vollum Institute for Advanced Biomedical Research

Craig Jahr, Ph.D., Senior Scientist, Dissertation Chairman
Vollum Institute for Advanced Biomedical Research

Marc Freeman, Ph.D., Senior Scientist and Director
Vollum Institute for Advanced Biomedical Research

Show-Ling Shyng, Ph.D., Professor
Department of Biochemistry and Molecular Biology

Ben Emery, Ph.D., Assistant Professor
Jungers Center for Neuroscience Research

TABLE OF CONTENTS

Table of content.....	3
Acknowledgements.....	4
Abstract.....	5-6
Chapter 1: Introduction.....	7-34
Chapter 2: Materials and Methods.....	35-42
Chapter 3: Astrocyte-neuron signaling in wildtype cortex.....	43-84
Chapter 4: Astrocyte-neuron signaling in MeCP2 null cortex.....	85-106
Chapter 5: The role of calcium in astrocyte-neuron signaling.....	107-121
Chapter 6: Discussion.....	122-135
Summary.....	136
References.....	137-151

Acknowledgements

I would first and foremost like to thank my two mentors, Paul Brehm and Gail Mandel. This work would not have been possible without their constant support and direction. They both always held me to a high standard and inspired my dedication to science. To PB, I will miss our conversations, jokes, and of course bagels. To Gail, I will also miss our conversations and your advice on life outside of lab. They truly made my graduate education an experience I will never forget.

I would also like to thank the members of the Brehm lab: Nathan, Hua, and Sarah, and the Mandel lab: Jon, Mike, James, Susan, Saurabh, and Justine. They have all provided me with a nurturing and fun environment, where we could talk about science and life. I must also thank Dan Lioy, who inspired this project and taught me that you have to stay true to your heart.

To my committee, I would like to thank their unyielding support and direction to ensure the progress of this project. Specifically I would like to thank Craig Jahr, who always offered insight into my experiments and reminded me to “always do the experiments that make you sweat”. I will never forget the help you have given me.

I would also like to thank my parents, Jorge and Rosa-Maria Rakela. They have always taught me to follow my dreams and have supported me throughout my years of education. I truly would not have been able to achieve all that I have without them. Thank you.

Abstract

Astrocyte-mediated processes are important for maintaining neuronal homeostasis and proper synaptic transmission. Recent work from the Mandel lab has implicated astrocytes in the X-chromosome linked autism-like spectrum disorder Rett syndrome (RTT), where global mutations in the methyl DNA-binding protein MeCP2 result in dysregulation of neuronal processes and severe mental retardation. Using paired recordings of astrocytes and neurons in cortical slices (p10-p12) I have shown that stimulation of wild type astrocytes using either depolarization or agonist application leads to potent activation of excitatory signaling in neighboring neurons involving both glutamatergic and GABAergic components. Interestingly, this astrocyte-mediated increase in excitatory neuronal signaling was greatly reduced when astrocyte stimulation was repeated in MeCP2-null mice, a mouse model for RTT. To determine whether this lack of astrocyte-mediated signaling was due to the astrocyte, the neuron, or both cell types being MeCP2 deficient, I took advantage of a MeCP2-GFP knock-in mouse line where female mice have mosaic expression of MeCP2 fused to GFP. The four combinations of paired-recordings between wild type and mutant astrocytes and neurons show that deficits in astrocyte-mediated neuronal signaling occurred when a MeCP2-deficient astrocyte was stimulated regardless of neuronal MeCP2 expression. These results indicate that the expression of MeCP2 in astrocytes is required for astrocyte-mediated modulation of neuronal signaling.

Further experimentation has identified that the defective signaling by MeCP2-deficient astrocytes involves aberrant astrocytic intracellular calcium

signaling. Calcium imaging of somatic calcium signals elicited by agonist application found reduced calcium responses in MeCP2-null astrocytes compared to wild type astrocytes. Furthermore, calcium imaging found no difference in calcium responses between MeCP2-null neurons and wild type neurons, indicating a specific deficit in MeCP2-null astrocytes. In an effort to restore astrocyte-mediated signaling in MeCP2-null astrocyte-neuron pairs, calcium uncaging was used. Surprisingly, photolysis of MeCP2-null astrocytes loaded with caged calcium did not reproduce the modulation of neuronal signaling found when photolysis was carried out in wild type astrocytes loaded with caged calcium, indicating that the deficit in MeCP2-null astrocytes is either downstream of calcium signaling or is affecting cellular processes not involving calcium. These data provide further support for the idea that astrocytes participate directly in the functioning of neuronal networks and that this astrocytic component is deficient in Rett syndrome.

Chapter 1

Introduction

Preface

The cerebral cortex is comprised of different cell types that culminate into an elegant network. Whereas synaptic transmission between neurons is the basis for processing afferent and efferent information, non-neuronal glial cells are critical for establishing and maintaining these circuits. Of the glial cells in the cortex, astrocytes are the most abundant (Lobsinger and Cleveland, 2007) and provide not only essential trophic and structural support (Stipursky et al., 2012) but also are now accepted as active participants in signal processing (Hamilton and Attwell, 2010). Given that astrocytes are capable of proliferation (Horner et al., 2000) and that a single cortical astrocyte enwraps between 4 and 8 neuronal somas and contacts 300-600 neuronal dendrites (Halassa et al., 2007), the potential for both local and global influence of astrocytes is substantial. Of particular interest however is the intimate relationship between one astrocyte and a neighboring neuron, and how astrocytic manipulation affects neurons in healthy and disease states.

The impetus for this research came from two discoveries from the Mandel lab that described a role for astrocytes in the neurodevelopmental disorder Rett syndrome (RTT), where loss of the methyl DNA-binding protein MeCP2 gives rise to severe neurological phenotypes. When wild type (WT) hippocampal neurons were co-cultured with astrocytes from RTT mice, there were apparent neuronal

morphological defects compared to those that were cultured with WT astrocytes (Ballas et al., 2009). Specifically, the WT neurons lacked fine processes and had fewer long processes, indicating that RTT astrocytes could not promote normal neuronal growth. Furthermore, conditioned media from RTT astrocytes also failed to promote normal neuronal growth in terms of dendritic morphology and neuronal density. These data were the first to suggest a non-cell autonomous interaction between astrocytes and neurons in RTT. The relevance of RTT astrocyte-neuron interaction was further tested by expressing MeCP2 in the astrocytes of a global null mouse. The expression of MeCP2 in astrocytes alone, *in vivo*, significantly improved locomotor skills and anxiety levels, rescued respiratory abnormalities to a normal pattern, and greatly prolonged survival compared to global null mice (Lioy et al., 2011). Though these data indicate an astrocytic component to RTT, the cellular mechanism for the astrocyte-neuron interaction has remained elusive. For this purpose, I have used electrophysiological recordings and calcium imaging to study the signaling between astrocytes and neurons in barrel cortex slices from healthy mice and from RTT mouse models.

Astrocytes: from glue to the tripartite synapse

The astrocyte was first described as being a component of the “nerve-glue” by Rudolf Virchow in 1856, but soon began to stand alone with the advancements of Ramon y Cajal who described their morphological diversity (1897). Surveying their morphology and location within the brain, Ramon y Cajal divided astrocytes into two main subtypes, protoplasmic and fibrous. Where protoplasmic astrocytes are located amongst the cell bodies of neurons in the grey matter of the brain, fibrous astrocytes are located amongst the axonal tracks of neurons in the white matter (Ramon y Cajal, 1909). The application of electron microscopy detailed how each subclass of astrocyte interacts with proximal neurons, with the protoplasmic processes enveloping synapses and the fibrous contacting the nodes of Ranvier on axons (Peters et al., 1991). Given the focus of this thesis on the astrocyte-mediated modulation of neuronal signaling in the cortex, the *protoplasmic* astrocyte is the protagonist for the following work.

The interaction between astrocytes and neurons is predicated on the astrocyte’s spatial domain. Staining for astrocytes reveals that in the cortex each astrocyte has its own territory, a spatial domain, endowing autonomous rule over neighboring neurons. Though astrocytes are coupled into a network connected via gap junctions (Axelsen et al., 2013), the activity of the astrocyte within its spatial domain has been thoroughly discussed (Mitterauer, 2010; Halassa et al., 2007; Oberheim et al., 2006, Oberheim et al., 2008). For example, the most contentious form of astrocyte-neuron signaling includes the “tripartite” synapse, where the functionality of the astrocytic processes enwrapping the synapse between pre-

synaptic terminals of neurons and post-synaptic dendrites are capable of modulating synaptic transmission (Araque et al., 1999). Another well-characterized form of astrocyte-neuron signaling includes the “neurovascular unit”, where astrocytes participate as a feedback loop with the vasculature of the brain. Neurovascular coupling is facilitated by astrocytic processes that ensheath blood vessels and maintain the integrity of the blood brain barrier. Signaling from the blood and from neurons is encoded by astrocytes to maintain the balance of nutrient entry and the release of waste (Abbott et al., 2010). Furthermore, astrocytes have been shown to be involved in several other critical processes to ensure an amenable environment for neurons: neurotransmitter reuptake and recycling (glutamate, GABA and glycine reuptake and clearance from the synaptic cleft) (Sattler and Rothstein, 2006; Nägga et al., 1999; Zhang et al 2008, respectively), potassium buffering (maintaining a low extracellular potassium concentration through the $\text{Na}^+\text{-K}^+\text{-ATPase}$, the NKCC cotransporter, and spatial buffering through the astrocytic network) (Bellot-Saez et al., 2017), glycogen storage (during hypoglycemia astrocytic glycogen is accessed to produce lactate for neurons to use as aerobic fuel, known as the “lactate shuttle hypothesis”) (Pellerin and Magistretti, 1994; Brown and Ransom, 2007) and reactive astrogliosis (protective response to trauma resulting in the sequestration of damaged areas via formation of the glial scar) (Sofroniew, 2009). These processes cement the importance of the astrocyte in promoting healthy neuronal function.

The majority of astrocyte-to-neuron signaling is contingent upon rises in astrocytic intracellular calcium. Astrocytes express various receptors for different

transmitters that convene on increasing intracellular calcium, namely G_q-coupled metabotropic receptors (mGluR5, P2Y, PAR, GABA_B) and ionotropic receptors permeable to calcium (NMDA, P2X, TRP, α7nACh). Activation of these receptors and the subsequent increase in intracellular calcium occur from exposure to neurotransmitters, mechanical stimulation, osmotic challenge, and spontaneous activity (Verkhratsky et al., 2014). The relevance of these astrocytic calcium signals to neuronal signaling has been a point of great controversy for some time. Evidence for glutamate-induced intracellular calcium signals and the propagation of calcium waves between astrocytes (Cornell-Bell et al., 1990; Dani et al., 1992; Porter and McCarthy, 1996; Newman and Zahs, 1997; Wang et al., 2006) was evidence that a neurotransmitter could initiate non-neuronal, astrocytic signaling. This rise in astrocytic intracellular calcium was then linked to the release of “gliotransmitters” that could in turn trigger neuronal calcium signals (Parpura et al., 1994; Nedergaard, 1994). This concept of “gliotransmission” has been shown to be initiated by glutamate, GABA, endocannabinoids, uncaging of calcium, uncaging of inositol-1,4,5-triphosphate (IP₃), synthetic peptides, and CO₂ blood levels. Reported “gliotransmitters” include glutamate (Parpura et al, 1994), ATP (Newman, 2003), D-serine (Yang et al., 2003), GABA (Jo et al., 2014), and derivatives of arachidonic acid (prostaglandins, epoxyeicosatrienoic acid, and 20-hydroxyeicosatetraenoic acid) (Zonta et al., 2003). The mechanisms by which gliotransmission occurs has also been a point of contention, with evidence supporting both canonical and non-canonical release mechanisms. The evidence for vesicular exocytosis (canonical) is based on electron microscopy studies that have identified the presence of small

vesicles (~30nm) in astrocytes resembling those found in neurons (Bezzi et al., 2004), and, at least for the canonical release of glutamate, immunocytochemical labeling of vesicular glutamate transporters 1 and 2 (VGLUT1 and VGLUT2) has been reported in GFAP⁺ astrocytes (Jourdain et al., 2007; Zhang et al., 2004; Montana et al., 2004). However, transcriptome and other immunocytochemical studies have been found to contradict these findings, with no detection of glutamate vesicular transporters in astrocytes (Cahoy et al., 2008; Franke et al., 2006). Additional evidence for canonical, vesicular-based gliotransmission came from the generation of a transgenic mouse line where exocytotic machinery was inhibited (only a portion of the SNARE molecule VAMP2 was expressed) in astrocytes. Inhibiting SNARE-mediated exocytosis in astrocytes was found to block synaptic transmission of ATP and impair neuronal plasticity by preventing LTP in hippocampal slices, indicating that astrocytes release ATP and are involved in LTP induction (Pascual et al., 2005). The specificity of these results was subsequently called into question when the transgene was also found to target VAMP2 in neurons, which confounds the conclusion that *astrocytic* ATP modulates synaptic transmission and LTP plasticity (Fujita et al., 2014). Additional experiments where microinjection of botulinum toxin (a SNARE-cleaving toxin) into astrocytes reduced the release of glutamate indicate that there is still ample evidence for an astrocytic canonical release mechanism (Araque et al., 2000). Non-canonical release mechanisms seem to be more widely accepted, including: reversal of glutamate and GABA reuptake transporters in slice recordings (Rossi et al., 2000; Wu et al., 2007), ATP and glutamate permeation through the large conductance pore of the P2X₇

receptor *in vitro* and *in situ* (Virginio et al., 1999), release of glutamate and ATP through hemichannels *in vitro* and *in vivo* (Stout et al., 2002), the release of glutamate through swelling-activated anion channels *in vitro* and *in vivo* (Seki et al., 1999), and the release of GABA through the bestrophin 1 channel *in vitro* (Lee et al., 2010). Conveniently, some of these release mechanisms can be activated through intracellular calcium, unifying canonical and non-canonical pathways (Mongin et al., 2005; Lee et al., 2010).

Given the wealth of literature implicating astrocytes in neuronal signaling, I have chosen three papers that focus on astrocyte-mediated processes in barrel cortex.

Perez-Alvarez et al., 2014, investigated how the structural relationship between astrocytic processes and neuronal dendritic spines change under conditions of experience-dependent plasticity. The authors utilized *in vivo* imaging of mouse barrel cortex layer 5 pyramidal neuron dendrites and sulforhodamine 101 (SR101) positive peridendritic astrocytic processes (PDAPs that were within 5 μ m of dendritic spines). The authors also imaged the calcium dynamics of the astrocytes in response to sensory stimuli. First, it was confirmed that whisker stimulation induced long-term potentiation (LTP) in the layer 5 pyramidal neuron circuit, indicating that the stimuli was potent enough to induce plasticity. The authors then reported that within 30 minutes of whisker stimulation PDAP motility increased (6% of PDAPs moved \sim 0.4 μ m). In addition, this sensory stimulation also resulted in increased intracellular calcium levels in the soma of astrocytes as well as in astrocytic processes. These astrocytic calcium signals were found to be IP₃-

mediated because repeating whisker stimulation in a mouse that lacks access to intracellular stores (IP₃R2^{-/-}) abolished the signaling. The authors then linked the PDAP motility to activation of astrocytic group I mGluRs and access to intracellular stores of calcium, because treatment with either mGluR antagonists MPEP/LY367385 or repeating whisker stimulation in IP₃R2^{-/-} mice blocked sensory stimulation-induced PDAP motility. These data suggest that as sensory information enters somatosensory cortex and increases glutamate-mediated signaling, astrocytes will respond to glutamate with mGluR-mediated increase in intracellular calcium that initiates PDAP motility. Though this publication did not directly address the functional significance of PDAP motility in somatosensory cortex, the authors postulate that their results may account for changes in synaptic regulation by astrocytes (i.e.: glutamate re-uptake and engulfment of weak synapses). Considering that the majority of *in vivo* imaging studies focus on the structural dynamics of neurons as they undergo experience-dependent plasticity, this publication was useful in elucidating the structural manifestation of astrocytic plasticity.

Min & Nevian, 2012 used electrophysiological recordings and calcium imaging of astrocyte-neuron pairs in layer 2/3 barrel cortex slices from young rats (p16-p21) to show that astrocytes participate in spike timing-dependent depression (t-LTD). This form of plasticity in barrel cortex, which is achieved by pairing excitatory postsynaptic potentials with a preceding postsynaptically evoked action potential (AP-EPSP), has been shown to require the activation of cannabinoid CB₁ receptor (CB₁R) and presynaptic NMDA receptors. The authors invest the entirety of

the study to show that astrocytes fulfill each aspect of these requirements. They postulate that astrocytes provide an ideal solution to how this form of plasticity is achieved, being that astrocytes express CB₁R, release glutamate, and have been found to make contact with pre-synaptic and post-synaptic neuronal compartments. The authors first established that stimulation of layer 4 afferents resulted in layer 2/3 astrocyte calcium signals, though this astrocyte response required concomitant depolarization of proximal neurons (AP-EPSP). These astrocyte calcium signals were found to be evoked by the postsynaptic neuronal release of the endocannabinoid 2-arachidonoyl glycerol (2-AG), given that CB₁R antagonist AM251 blocked the effect. The authors then blocked astrocyte calcium signaling by including calcium buffers in the patch pipette, which was effective in blocking the astrocytic calcium responses to AP-EPSP pairing and was also found to block t-LTP induction. Having shown that astrocyte calcium levels change in response to the t-LTP protocol and that astrocyte calcium is required for the plasticity, the authors then blocked vesicular exocytosis in astrocytes to determine its effect on t-LTP. Indeed, including tetanus toxin in the astrocyte patch pipette abolished t-LTP, indicating that this form of plasticity requires SNARE-dependent exocytosis from astrocytes. To identify the gliotransmitter mediating the t-LTD, the authors focused on molecules that activate NMDA receptors, being that NMDA receptors are required for t-LTD. D-serine was ruled out because exogenous application of D-serine had no effect on t-LTD, therefore the authors focused on glutamate. The astrocytic vesicular release of glutamate was inhibited by targeting the vesicular transporter for glutamate (VGLUT), which the authors claimed to have achieved by

including Evans Blue or high chloride in the internal solution. The inhibition of astrocytic VGLUT was then found to significantly reduced t-LTD. At this point the authors offer a model for their effect: upon depolarization of a proximal neuron, endocannabinoids are released which retroactively activate astrocyte calcium signaling which results in the exocytosis of glutamatergic vesicles which then activates pre-synaptic NMDARs to carry out t-LTD. The direct evidence for astrocyte involvement was finally achieved by directly depolarizing astrocytes to determine if synaptic depression was induced in a proximal neuron. Interestingly, depolarizing astrocytes only produced LTD (astrocyte-LTD; a-LTD) in the proximal neuron when layer 4 afferents were also stimulated, further indicating that multiple inputs are required to drive astrocyte-mediated effects. The authors go on to show that a-LTD required activation of NMDA receptors (effect was blocked with NMDAR antagonist AP5), and was downstream of endocannabinoid signaling (AM251 had no effect on a-LTD). Overall this study indicates that astrocytes serve as coincidence detectors in the circuit; astrocyte activation was achieved after correlated neuronal activity built up enough endocannabinoid signal required to recruit the astrocyte. This also inherently implies astrocytes function at a slower rate, on the timescale of minutes, which also calls into question its relevance for the immediate processing of sensory stimuli. Though this paper does implicate astrocytes in barrel cortex t-LTD, some of the experiments, and their interpretations, call for closer examination. For example, the astrocyte calcium-buffering experiments were interpreted as evidence for astrocyte calcium being required for t-LTD, although only 56.9% of astrocytes showed calcium transients during the t-LTD induction protocol. If astrocyte calcium

is required for this effect, one would assume more astrocytes would be responding to the induction. Second, astrocytic vesicular exocytosis is extremely contentious; though other groups have reported similar findings that tetanus toxin treatment abolishes astrocyte-mediated effects, it is suspicious that there were no residual effects given that non-canonical (non-vesicular) release mechanisms are so well characterized in astrocytes. Third, the block of VGLUT with evens blue and the high chloride internal is also problematic being that neither of these treatments is specific for VGLUT. Fourth, the depolarization-based a-LTD required astrocyte depolarization for a 10-minute period, which at best is non-physiological and at worst is damaging the astrocyte. Nevertheless, this publication was an extensive study on the involvement of astrocytes in neocortical plasticity.

Benedetti et al., 2011 utilized electrophysiological astrocyte-neuron recordings in mouse barrel cortex slices to study how astrocytes modulate inhibition within a sensory column (barrel field). Previous data from this lab found that in barrel cortex slices, extracellular electrical stimulation evoked calcium responses in astrocytes when they were located within the stimulated barrel field (Schipke et al., 2008) and that these astrocytic calcium signals depended on neuronal activity as they were blocked by tetrodotoxin. The relevance of these astrocytic calcium signals to neuronal activity was studied by blocking astrocytic calcium signaling with BAPTA and determining the subsequent impact on neighboring neurons. First, the authors report that neuronal EPSPs can be evoked in layer 4 and 2/3 with a stimulating electrode (~30mV depolarization), and that after including BAPTA in the astrocyte patch pipette and repeating extracellular

stimulation, the EPSPs in proximal neurons were larger (~40mV depolarization) and longer (half repolarization increased by ~1 sec). Furthermore, dialyzing astrocytes with BAPTA also increased the frequency of spontaneous synaptic activity in proximal neurons. Taken together these data suggest that blocking astrocyte signaling leads to increased excitation. In order to explain how blocking astrocyte calcium signaling had this effect, the authors repeated extracellular stimulation in the presence of different pharmacological antagonists to determine if drug treatment resulted in similar augmentation of the EPSP (GABA_A antagonist gabazine, GABA_B antagonist CGP55845, AMPAR/kainate antagonist CNQX, NMDAR antagonist AP5, mGluR1-5 antagonist LY367385 and MPEP, glycine receptor antagonist strychnine, and purinergic receptor antagonist CPT). The combination of blocking both GABA_A and GABA_B was the only pharmacological treatment that resulted in similar effects on EPSPs, which the authors suggest indicates that astrocytes may be modulating GABAergic signaling. To further investigate whether astrocytes are releasing GABA, proximal neurons were dialyzed with a low chloride internal and clamped at -40mV (making GABA-mediated currents inhibitory). After extracellular stimulation the authors observed a hyperpolarization, although if the neuron was proximal to a BAPTA-dialyzed astrocyte, the authors observed a depolarization, which according to the authors is evidence that the astrocyte may be releasing GABA in a calcium-dependent manner. The authors also studied the spread of BAPTA within the astrocytic network, reporting that after 45-60 min of astrocyte dialysis, calcium signaling was shut down in all astrocytes within ~200µm (6-12 astrocytes). In conclusion, the authors determine that astrocytes contribute to

neuronal inhibition in barrel cortex through a calcium dependent mechanism potentially mediated by release of GABA and subsequent activation of both neuronal GABA_A and GABA_B. This paper, though thorough in its electrophysiological analysis of how neuronal physiology is affected by astrocytes, does not directly study astrocyte-modulation. The authors studied astrocytic contributions by silencing the astrocyte, rather than activating it. This indirect measure of how astrocytes modulate GABAergic signaling can only associate astrocytes in these effects, rather than prove their causality. In addition, there were some troubling caveats tucked away in the methods, for instance the BAPTA-internal solution for astrocytes included: (in mM) 90 potassium gluconate, 40 BAPTA, 1 MgCl₂, 8 NaCl, 2 ATP, 0.4 GTP, and 10 HEPES. In order to include this high concentration of BAPTA, the authors reduced the amount of potassium in the internal solution. Having a low intracellular potassium concentration would have a depolarizing effect and is also contrary to one of the main roles of astrocytes as a potassium sink. Furthermore, this amount of BAPTA would effectively strip every organelle of calcium and disrupt all basal processes that require resting calcium levels which undoubtedly has off-target effects and was not addressed in the publication. Considering these issues, the conclusions from this paper were based on the effect of silencing astrocytes in barrel cortex, which the authors have undoubtedly achieved. The most useful data from this publication is the spread of BAPTA within the astrocytic network, which serves as a warning that BAPTA-mediated effects will not be limited to one astrocyte.

These three publications each make the case that astrocytes are actively involved in the modulation of neuronal signaling and provide important contributions to neuronal circuits in barrel cortex. They suggest that astrocyte activation changes both the structural and chemical signaling between astrocytes and neurons, and identify glutamate and GABA as gliotransmitters in barrel cortex that are released through a calcium dependent mechanism.

Rett syndrome: a brief history

Rett syndrome (RTT) is a devastating neurodevelopmental disorder that is due to *de novo* mutations in the gene coding for the transcription factor methyl-CpG-binding protein 2 (MeCP2). *Mecp2* is on the X-chromosome, which means males who inherit an X-chromosome with mutated *Mecp2* are usually not viable or expire within the first year of life. Females, on the other hand, inherit one paternal and one maternal X-chromosome, and due to X-chromosome inactivation it is random which X-chromosome is expressed in a given cell. When a female is afflicted with RTT, X-chromosome inactivation endows the individual with mosaic expression of the mutant MeCP2, where 50% of cells will express the mutant form and 50% will express functional MeCP2. These individuals appear to develop normally up to 6-18 months of age and often begin to miss developmental milestones. Symptomatic phenotypes associated with RTT include: loss of purposeful hand movements with the development of stereotypic hand movements such as hand wringing and flapping, weight loss, and low muscle tone. Patients with RTT also experience cognitive phenotypes; they become socially withdrawn, lose any language that was

developed prior to symptom onset, and are plagued with irritability and anxiety. RTT is not a neurodegenerative disorder, these individuals survive into their sixties and seventies, though as they get older they begin to present with Parkinsonian symptoms. Generally, patients suffer extreme motor deterioration and rigidity that renders them wheelchair-bound. They also present with autonomic respiratory abnormalities including hyperventilation, breath-holding, forced expulsion of air, and apnea. One of the most burdensome phenotypes is seizure, which range in severity, with the most common type being partial complex and tonic-clonic seizures. Given all of this is due to mutations in just one gene, RTT has been of interest to biologists since the genetic basis was first discovered in 1999 in the lab of Huda Zoghbi (Amir et al., 1999).

MeCP2 was first discovered in 1992 by Dr. Adrian Bird, who described a novel mammalian protein that bound methylated CpGs (Lewis et al., 1992). The gene was localized to the X-chromosome and repressed transcription in vitro (Nan et al., 1997). More than 95% of classic RTT cases are due to mutations in *Mecp2*, which involve C to T transition at CpG dinucleotides and arise *de novo* in the paternal germline (Trappe et al., 2001; Wan et al., 1999). The gene has four exons, though exon3 and a portion of exon4 contain coding sequences. There are three domains that comprise the protein, the methyl-DNA binding domain (MBD), a transcriptional repressor domain (TRD) containing the NCOR-SMRT interaction domain (NID), and a C-terminal domain, in addition to two nuclear localization sequences (NLS). Mutations in these domains will give rise to RTT, though different mutations will affect the severity of the syndrome. Specifically, the RTT-causing

missense mutations in the MBD include: Arg106Trp, Arg133Cys, and Thr158Met. The TRD nonsense mutations include Arg255x and within the NID, Arg270X, Arg249X, and the missense mutation Arg306Cys. The most severe mutations include Arg270X, Arg255X and Arg168X, whereas Arg133Cys, Arg294X and C-terminal deletions produced less severe phenotypes (Leonard et al., 2017). The location of the mutation will affect the respective function of the gene, i.e.: mutations in the MBD will affect the proteins ability to bind methylated DNA, effectively rendering a loss of function. Over all, the phenotypic variability found in RTT is due to both the type of mutation and X-chromosome inactivation, but the neurological phenotypes unite all patients.

Rett syndrome mouse models

In order to study this syndrome, mouse lines have been developed that recapitulate the neurological phenotypes of the disease. Though human RTT afflicts females, both female and male mice are commonly used. Male *Mecp2* global knockout mice, lacking the coding regions (either exon 3 or exon 3 and 4), develop normally for a period of time but succumb quickly to the disease, leading to death at 8-10 weeks of age (Chen et al., 2001; Guy et al., 2001). Male mice (*Mecp2^{-y}*), though not a true representation of the disease, are often preferable because the female mice (*Mecp2^{+/-}*) develop behavioral abnormalities at a much slower rate and often survive for the entirety of their life. In addition to global null mice, mouse models with specific RTT-causing mutations have recently been created, including: Arg225X, Thr158Met, Thr158A, Arg306C, Arg133C, A140V, Arg111G, and Arg168X.

These mice are particularly useful when the research question involves the role of specific functional domains of MeCP2 and impart relevance to the human disorder.

Given the neurological phenotypes of patients with RTT, there has been a large effort to create mice that lack MeCP2 in the different cells that comprise the brain. Using a nestin-Cre transgene, an embryonic *Mecp2* deletion only in neurons resulted in a phenotype resembling the ubiquitous knockout, establishing that loss of MeCP2 in the brain is enough to cause RTT (Guy et al., 2001). Deletion from GABAergic neurons results in a near-complete RTT phenotype, including motor and cognitive impairments (Chao et al., 2010), whereas deletion in glutamatergic neurons reproduced the anxiety and tremor phenotypes (Meng et al., 2016). Furthermore, loss of *Mecp2* in post-mitotic neurons using a CaMKII- Cre transgene results in delayed and less severe neurological phenotypes (Chen et al., 2001), indicating a role of non-neuronal cells in RTT.

Arguably, the most powerful discovery to come from the RTT mouse models was proof that the disease is reversible. The most effective rescue came with global re-expression of *Mecp2* in a symptomatic adult mouse using an endogenous promoter (chicken beta-actin). The conditional re-expression of *Mecp2* in all cell types resulted in normal longevity, rescued motor abnormalities, and improved overall health of the mouse (Guy et al., 2007). Rescuing *Mecp2* in only postmitotic neurons using the *tau* promoter prevented the appearance of several RTT-like symptoms including tremors, gait ataxia, and side-to-side swaying (Luikenhuis et al., 2004), but did not represent a complete rescue. Interestingly, restoring the expression of *Mecp2* in astrocytes using an inducible cre-transgene driven by the

GFAP promoter significantly improved locomotor skills and anxiety levels, rescued respiratory abnormalities to a normal pattern, and greatly prolonged survival compared to global null mice (Lioy et al., 2011). Being that the global re-expression of *Mecp2* was more successful in reverting RTT phenotypes than the neuronal rescue, a role for glial cells in RTT cannot be overlooked.

A role for astrocytes in Rett Syndrome

The discovery that MeCP2 was expressed in glial cells was the first insight into the role of non-neuronal cells in RTT (Ballas et al., 2009; Skene et al., 2010; Rastegar et al., 2009; Kifayathullah et al., 2010). These findings were contentious because previous studies using commercial anti-MeCP2 antibodies to immunolabel mouse and primate tissue only detected MeCP2 in neurons (Akbarian et al., 2001). The expression of MeCP2 in glial cells, including astrocytes, was achieved with the use of either more efficient antibodies or enhancing the immunolabel using Biotin/Streptavidin (Ballas et al., 2009). In order to study the involvement of astrocytes in RTT, three general approaches have been taken, first, astrocytes from RTT mouse models have been cultured to study their effect on neurons *in vitro*, second, inducible pluripotent stem cells (iPSC) of human origin have been used to study how differentiated astrocytes affect neuronal processes *in vitro*, and, thirdly, the astrocytic expression of MeCP2 in a whole animal (mouse) has been manipulated *in vivo* to study associated phenotypes. Regardless of the approach, recent publications have implicated astrocytes in the progression of RTT.

The publication from *Ballas et al* (2009) used was the first to identify non-cell autonomous effects of MeCP2-deficient astrocytes on neurons. First, the loss of astrocytic MeCP2 was confirmed in the brains of RTT mice using immunolabeling and the functional loss of MeCP2 was confirmed by western blotting for the presence co-repressors associated with MeCP2. The authors reported that the reduction of H3K9me3 along with the elevated levels of acetylated histone H3 suggested that the loss of MeCP2 resulted in less recruitment of histone modifying enzymes, which could potentially shift the astrocyte into a more permissive state for gene expression. To determine if MeCP2 dysfunction in astrocytes can influence neurons, *Ballas et al* used a co-culture system where neurons are dependent on an astrocytic feeder layer for survival (Banker, 1980; Kaech and Banker, 2006). Interestingly, when MeCP2-expressing neurons (WT neurons) were cultured with MeCP2-null astrocytes (RTT astrocytes), the WT neurons had quantifiable differences compared to when they were cultured with WT astrocytes. Specifically, when WT neurons were cultured with RTT astrocytes, 40% of them had processes shorter than 50 μ m, compared to the 5% when WT neurons were cultured with WT astrocytes. Furthermore, these deficits appeared after 6 DIV, suggesting that MeCP2-null astrocytes cannot support normal neuronal development. To determine whether these deficits were due to the presence or lack of a soluble factor that was released from the astrocyte, *Ballas et al* treated neurons with astrocytic conditioned media (ACM) from RTT astrocytes. After 6 days in culture with ACM from RTT astrocytes, WT neurons exhibited the same stunted dendritic morphology found in the co-cultures. They found that up to 80% of WT neurons had abnormal dendritic

morphology when treated with ACM from RTT astrocytes, whereas only 10-15% of WT neurons had abnormal dendritic morphology when treated with ACM from WT astrocytes. Furthermore, mixing WT and RTT ACM in a 1:1 ratio also resulted in similar defects in dendritic morphology. The authors then did the complementary experiment, where RTT neurons were treated with ACM from WT astrocytes. RTT neurons appeared healthy when compared to treatment with ACM from RTT astrocytes, which resulted in aberrant dendritic morphology. Specifically, 70% of RTT neurons had short dendrites when cultured in RTT ACM, but only 10% of RTT neurons had short dendrites when cultured in WT ACM. These data were the first to suggest a non-cell autonomous interaction between MeCP2-null astrocytes and neurons, indicating that in the brains of RTT patients, where 50% of astrocytes are MeCP2 deficient and the other 50% express MeCP2, the lack of MeCP2 in astrocytes has detrimental effects on the MeCP2-expressing neurons. Though this was a seminal publication in terms of implicating astrocytes in RTT, the application to the human disease is still limited given these are non-human derived cells and the interaction between astrocytes and neurons was investigated in culture.

Williams et al used an *in vitro* human RTT model to study how loss of MeCP2 in astrocytes affects their interaction with neurons. The authors differentiated isogenic pairs of RTT iPSC lines carrying several RTT-causing mutations (V247X, R294X, R306C) into GFAP⁺ “astrocytes”. After validating that the iPSC lines maintained their original isogenic status, the authors demonstrated that these human-derived RTT “astrocytes” had adverse effects on the morphology and function of WT mouse hippocampal neurons *in vitro* compared to culturing the WT

neurons with MeCP2-expressing astrocytes. The data supported previous work (*Ballas et al.*) in that WT neurons co-cultured with RTT astrocytes had significantly smaller soma size, shorter total neurite length, and fewer synaptic terminals. Furthermore, the media from these RTT astrocytes produced similar effects. Next, the authors addressed the mosaicism that exists in the brain of RTT patients. To model the interaction between MeCP2 positive and negative cells, the authors differentiated the same isogenic pair of RTT iPSC lines into GABAergic interneurons and astrocytes. The four co-culture combinations (WT interneuron/ WT astrocyte, WT interneuron/ RTT astrocyte, RTT interneuron/ WT astrocyte, RTT interneuron/ RTT astrocyte) found that the total neurite length and the number of neuronal terminals in WT interneurons was reduced when they were cultured with RTT astrocytes and that WT astrocytes could rescue these effects in RTT interneurons. The authors then sought to test two potential RTT therapies on the co-cultures. Insulin-like growth factor 1 (IGF-1) and GPE (a peptide containing the first 3 amino acids of IGF-1) have been shown to partially rescue RTT-like phenotypes in MeCP2-null mice. Interestingly, GPE was more effective than IGF-1 in rescuing total neurite length when either WT or RTT interneurons were cultured with RTT astrocytes. The effect of either treatment on the number of neuronal terminals was negligible, and, IGF-1 treatment had a negative effect on the total neurite length and number of terminals in both WT interneuron/ WT astrocyte and RTT interneuron/ WT astrocyte combinations. The authors settled with the conclusion that the direction of IGF-1/GPE treatment depended on the genotype of the astrocyte, with benefits occurring when the astrocyte was MeCP2 deficient. Overall, the use of human-

derived cells, the use of different human-RTT-causing mutations in the generation of the RTT cells, and the application of current RTT therapies helps this paper bridge the gap RTT mouse models and human RTT.

Delépine et al combined the use of primary culture of astrocytes from RTT mouse models and the generation of human-derived astrocytes to study how the loss of MeCP2 affects astrocytic intracellular processes. Specifically, the authors looked at microtubule (MT) dynamics and vesicular transport in these cells. The stability of MTs, which is regulated by acetylation, is critical for cellular functions (migration, division, polarity, and differentiation) and the trafficking of vesicles. The authors reported that RTT astrocytes (mouse and iPSC) had low level of tubulin acetylation and overexpression of HDAC6, an enzyme shown to deacetylate α -tubulin, suggesting MT instability. They also show that MT-dependent vesicle transport was altered in both human-derived and mouse RTT astrocytes, in that the percentage of highly direction vesicles was reduced when compared with WT astrocytes. The authors then sought to correct this deficit by treating astrocytes with Epothilone D (EpoD), a compound shown to stabilize MT. Their data show that EpoD treatment rescued both MT growth velocity and vesicle directionality, and, when RTT mice were treated with EpoD, exploratory behavioral symptoms were corrected. This paper is the first to find a specific cellular defect within the astrocyte that could be a viable target for therapeutic intervention. The finding that astrocyte MT-destabilization leads to altered vesicle trafficking is relevant to the previous publications that reported RTT astrocytes do not support normal neuronal development, because it offers a mechanism for the reduction of pro-growth

astrocyte factors. However, for these data to apply, these astrocyte factors would have to follow canonical vesicular release.

The most conclusive evidence for whether astrocytes play a role in Rett syndrome came with the publication by *Lioy et al* (2011), where MeCP2 was re-expressed in the astrocytes of a MeCP2-null animal. This was achieved by crossing a mouse containing a transgene expressing a tamoxifen (TAM)-inducible cre recombinase (*creT2*) under the control of a human astrocytic glial fibrillary acidic protein promoter (*hGFAP*) (Hirrlinger et al., 2006) with a RTT mouse containing an excisable transcriptional *stop* sequence in the *Mecp2* gene (Guy et al., 2007), such that treatment with TAM would activate *cre* to remove the *stop* in MeCP2 in astrocytes alone. This mouse could then be used to directly identify what RTT phenotypes are associated with the astrocytic expression of MeCP2. The authors found that when MeCP2 was re-expressed in astrocytes, *in vivo*, there was significant improvement in locomotor skills and anxiety levels, respiratory abnormalities were rescued to a normal pattern, and astrocyte-rescue mice had prolonged survival compared to global null mice. Furthermore, the authors found that when MeCP2 was expressed in astrocytes alone, *in vivo*, the dendritic morphology of RTT neurons was restored to normal levels by 3.5 months (without restoring astrocytic MeCP2, RTT mice had ~25% less total number of apical dendrite branches compared to controls). They also found that restoring MeCP2 to astrocytes alone supported neurotransmission; in the RTT mouse there was ~20% less peri-nuclear VGLUT1 staining, but after re-expressing MeCP2 in astrocytes, this level increased to normal by 3-4months. An important caveat to this publication,

with regards to the rescue of RTT phenotypes, is the amount and location of astrocytic MeCP2 expression. With TAM treatment, only caudal brain regions were found to express levels of astrocytic MeCP2 over 60% (cortex only found ~15% expression). The brain regions that saw increased expression of MeCP2 in astrocytes were also the brain regions involved in the phenotypes that were rescued: cerebellum (locomotor skills) and brain stem (respiration) being the highest. It would be interesting to see if additional phenotypic rescue could be achieved by expressing MeCP2 in cortical astrocytes. Nevertheless, these data indicate that re-expression of MeCP2 in astrocytes ameliorates RTT-like phenotypes in mice, and implicates astrocytes in both non-cell autonomous effects and behaviors such as locomotion and breathing.

Garg et al took a closer look at how astrocytes are involved in the respiratory abnormalities that are present in RTT mice and RTT patients. The role of astrocytes in the mechanisms controlling breathing has been well characterized. Astrocytes at the ventral surface of the medulla oblongata have been shown to be sensitive to changes in the ratio of CO₂/pH, where they contribute to ATP-mediated adaptive increases in breathing when CO₂ levels are elevated in the blood (Gourine et al., 2010). Given that patients with RTT and RTT mouse models present with several respiratory abnormalities and that *Lioy et al* have shown that restoring MeCP2 to astrocytes in a null animal improves respiratory abnormalities, the authors of this paper demonstrated that the loss of astrocytic MeCP2 *in vivo* is sufficient to dramatically attenuate the response to elevated CO₂ levels (hypercapnic ventilatory response- HCVR). This was achieved by crossing a mouse containing a transgene

expressing a tamoxifen (TAM)-inducible cre recombinase under the control of a human astrocytic glial fibrillary acidic protein promoter (*hGFAP*) (Hirrlinger et al., 2006) with a RTT mouse containing an excisable third exon of the *Mecp2* gene (Chen et al., 2007), such that treatment with TAM would activate *cre* to remove the third exon of MeCP2 in astrocytes alone, rendering them null. When MeCP2 was lost in 80% of astrocytes in the brain regions involved in CO₂-mediated respiration (retrotrapezoid nucleus and the raphe magnus) there was a significant depression of the ventilatory response to increases in the level of inhaled CO₂. This reduction (43, 59, and 62% less than WT at 5, 3, 1 % inspired CO₂) was similar to that found in the mice that were globally MeCP2-null and was comparable to studies where respiratory neurons were silenced (Hodges & Richerson, 2008). These data indicate that astrocytes play a major role in adapting ventilation to account for increases in CO₂. As a possible mechanism, the authors postulate that this effect may be due to reduced astrocytic expression of Kir4.1 with loss of MeCP2, this potassium channel that has been associated with depressed CO₂ chemosensitivity and is found to be reduced in RTT astrocytes when compared to WT astrocytes. The loss of astrocytic MeCP2 in this publication, along with the gain of astrocytic MeCP2 in *Lioy et al*, offer both perspectives for the importance of astrocytic MeCP2 in normal respiration, although the exact cellular mechanism for the rescue and attenuation remain elusive.

The publication by *Turovsky et al* (2015) is similar to the *Garg et al* (2015) study in that the authors sought to elucidate how astrocytic responses to CO₂ were affected in Rett syndrome. Specifically, *Turovsky et al* used brainstem slices from

MeCP2 null mice to determine whether the metabolic activity of MeCP2-deficient astrocytes in the ventral medulla oblongata (the brain area responsible for regulating respiration) is compromised and whether these astrocytes are capable of responding to stimuli via calcium signaling. First, using a lactate biosensor, the authors report that the tonic lactate tone in the ventral surface of the brainstem was no different between WT and MeCP2-null mice. The lactate biosensor measures the release of lactate using an amperometric biosensor, which is placed in direct contact with the surface of the slice. The measurement of lactate is indirect, the biosensor uses lactate oxidase, which in the presence of oxygen, converts lactate to pyruvate and H_2O_2 which can be detected electrochemically. The difference in biosensor current between lactate and no-lactate conditions was then used to determine the amount of lactate release. Using this sensor, the authors then applied hypoxic stress to the slice, which increases the production and release of lactate. The amount of lactate released in response to the hypoxic challenge was also no different between WT and MeCP2-null mice. These data indicate that glycolysis in astrocytes is not affected by the loss of MeCP2 and that the lactate transporter (MCT) is also functional. Though the astrocyte “lactate shuttle” was found to be intact in RTT mice, there was a dramatic reduction in intracellular calcium responses to increased CO_2 levels (10% CO_2). As previously mentioned, CO_2 -evoked calcium signals in astrocytes results in the release of ATP, which contributes to the excitation necessary to drive adaptive increases in the neuronal respiratory network. The reported attenuation of RTT astrocyte calcium signals to CO_2 would directly implicate astrocyte calcium signaling in the RTT respiratory abnormalities.

However, the astrocytes that did not respond to 10% CO₂ could be driven to produce calcium signals when exposed to extreme levels of CO₂ (23%). Furthermore, the authors found that RTT astrocytes produced normal calcium signals in response to direct application of ATP. Taken together, these data show that loss of MeCP2 does not affect intracellular calcium signaling, however the ability to sense changes in CO₂ is affected. This blunting of astrocytic CO₂ sensitivity may explain why patients with RTT are capable of respiration but with irregularities.

Though the loss of MeCP2 in neurons is still considered to be the basis of RTT, these publications have built a convincing case for astrocytes in many of the phenotypes associated with RTT. Furthermore, these data also identify different aspects of astrocyte-neuron signaling that are relevant to this dissertation, namely the reduction in the release of astrocytic factor(s), aberrant calcium-dependent vesicular release, deficient calcium responsiveness, and c astrocyte-neuron signaling in the mosaic, RTT female brain.

Significance

The goal of this thesis is to understand how astrocyte-mediated modulation of neuronal signaling is affected by the loss of MeCP2. Given the previous studies that have identified non-cell autonomous effects between RTT astrocytes and neurons and that RTT phenotypes can be ameliorated by restoring MeCP2 in astrocytes, this work addresses the unknown underlying cellular mechanism. By first characterizing the signaling between wild type cortical astrocytes and neurons using electrophysiology and calcium imaging, I hope to identify aberrant processes that may serve as potential targets for therapeutic intervention in Rett syndrome. Overall, the study of astrocyte-mediated modulation of neuronal signaling in both a healthy and a disease state offers a unique opportunity to address both the dynamic relationship between astrocytes and neurons and to identify the effect of losing astrocytic contributions.

Chapter 2

Materials and Methods

Animals:

All animal procedures used in this study were approved by the Oregon Health and Science University Institutional Animal Care and Use Committee. Mice were kept on a 12 hour light/dark cycle and were housed with their littermates. Three genotypes were used in this study: C57BL/6J,, *Mecp2^{tm1.1Bird}* (*Mecp2^y*; catalog 003890; Guy et al., 2001), and *Mecp2^{tm3.1Bird}* (*Mecp2^{EGFP}*; catalog number 014610; Lyst et al., 2013). All mice were obtained from Jackson Laboratory and crosses were maintained on a C57BL/6J background for X generations. Mice were genotyped by PCR as described previously (Lioy et al., 2011; Lyst et al., 2013). To generate heterozygous *Mecp2^{Bnull/EGFP}* females (mice carrying a *Mecp2-EGFP* allele and a germ-line *Mecp2*-null mutation,), *Mecp2^{EGFP/y}* male mice were crossed to heterozygous *Mecp2^{Bnull/+}* mice.

Brain slice preparation:

Mice between ages p10 and p12 were anesthetized with isoflurane prior to decapitation and removal of the brain. Coronal slices (200 μ m) were cut from the barrel cortex of the right hemisphere using a vibratome (Leica VT1200s). An ice-cold cutting solution contained: (in mM) 110 CholineCl, 2.5 KCl, 1.25 NaH₂PO₄, 1.3 Na-ascorbate, 3 Na-pyruvate, 10 glucose, 25 NaHCO₃, 0.5 CaCl₂, 7 MgCl₂ and adjusted to pH 7.3. Slices were then placed in a recovery solution for 35 minutes at

~35°C which contained: (in mM) 119 NaCl, 2.5 KCl, 1 NaH₂PO₄, 1.3 Na-ascorbate, 3 Na-pyruvate, 10 glucose, 26 NaHCO₃, 1.5 CaCl₂, 1 MgCl₂ and 100 nM SR101 to label astrocytes. The recovery solution was continuously bubbled with Carbogen (Carbon dioxide 5%, balanced oxygen). Slices were then transferred to a lower temperature recovery solution (23°C) for an additional 35 minutes and used within 5 hours.

Electrophysiological recordings, analyses and statistics:

All recordings were performed at ~32°C from layer 2/3 barrel cortex astrocytes and neurons. Astrocytes and neurons were visualized by means of an IR-DIC 40x W achroplan objective using a Zeiss Axiocam MRm (Zeiss, Oberkochen, Germany). Astrocytes were identified on the basis of Sulforhodamine 101 red fluorescence (100nM, Sigma-Aldrich, St. Louis, MO). In MeCP2-GFP knock-in mice, expression of MeCP2 was identified on the basis of MeCP2-GFP fluorescence.

The extracellular recording solution contained: (in mM) 110 NaCl, 2.5 KCl, 1 NaH₂PO₄, 10 glucose, 26 NaHCO₃, 2 CaCl₂, and 1.3 MgCl₂. The recording solution was continuously bubbled with Carbogen to maintain the pH at 7.3. The internal solution for symmetrical chloride recordings contained: (in mM) 140 CsCl, 10 HEPES, 10 EGTA, pH 7.35. The internal solution for low intracellular chloride contained: (in mM) 130 K-Gluconate, 10 KCl, 10 EGTA, 10 HEPES, pH 7.38. For blocking intracellular calcium signaling, 10mM BAPTA was included in the patch pipette with the symmetrical chloride recording solution. For experiments where BAPTA was buffered, 4.83mM CaCl₂ was incubated with 10mM BAPTA and the symmetrical chloride internal solution was used. All recordings utilized a triple headstage EPC10 HEKA amplifier. Data was acquired using Patchmaster software

(HEKA elektronik, Lambrecht/Pfalz, Germany) at a sampling rate of 10kHz and Bessel filtered offline at 500Hz.

For perforated patch neuron recordings, the tip of the patch pipette was filled with gramicidin-free internal solution and backfilled with internal solution containing 100 μ g/mL gramicidin (Calbiochem, San Diego, CA). Following seal formation the resistance was monitored until it dropped to <50 megohm.

Establishment of the whole cell recording was then confirmed on the basis of a large voltage activated sodium current.

To deplete slices of vesicular contents, bafilomycin A1 was used (Calbiochem, San Diego, CA). Slices were cut as before and allowed to recover at 23°C for 40 minutes. After recovery from slicing, each slice was incubated in 2 μ M bafilomycin for 1 hour at 23°C before use.

For ATP dialysis experiments of MeCP2 deficient astrocytes, 5mM ATP was included in the patch pipette. Experiments were conducted after 15 minutes of ATP dialysis. Astrocyte activation was carried out using 500 μ M TFLLR as before and the effect on neighboring neurons was determined. To determine if ATP was being used metabolically for intracellular process or being released by the astrocyte, the experiment was repeated in the presence of the purinergic receptor antagonist PPADS (100 μ M, Tocris, Bristol, UK), which was washed onto the slice for a minimum of 15 minutes.

Spike train averaging was used to determine if the appearance of neuronal synaptic currents was relevant to astrocyte activation. Astrocytes were depolarized at 1hz with one 20msec voltage step (-80mV to +120mV) while a neighboring

neuron was voltage clamped at -100mV using a symmetrical chloride internal. The timing of synaptic currents within a 200msec window following the astrocyte voltage step was compared to the frequency of currents 200msec before astrocyte stimulation. The astrocyte was stimulated at 1hz to avoid large-scale astrocyte mediated modulation of neuronal signaling found with stronger stimuli. Recordings were taken over 100 seconds and the data was pooled across 15 neurons.

The amplitude and time of occurrence for individual synaptic currents were determined using a combination of Patchmaster, ClampFit (Axon Instruments, Sunnyvale, CA) and Minianalysis software (Synaptosoft, Decatur, GA). After 500 Hz filtering the threshold for event detection was set to 3x RMS noise for symmetrical chloride recordings and to 2x RMS for low chloride internal solution recordings. Statistical analyses were carried out using GraphPad Prism6 software (La Jolla, CA). For paired t-test, the nonparametric test Wilcoxon matched-pairs signed rank test was used. For unpaired t-test, the nonparametric test Mann-Whitney test was used. If a parametric test was used, the normality of the distribution had to pass both the D'Agostino & Pearson omnibus normality test and the Shapiro-Wilk normality test. All t-tests were two-tailed and a confidence level of 95% was used. Statistical significance was determined if $P < 0.05$.

The agonists L-glutamic acid, TFLLR-NH₂, and GABA were pressure applied using a picospritzer (Parker Instruments, Boaz, Al) via a 5-micron tip puffer electrode. The pressure pulse duration was set to 500msec. The antagonists gabazine (SR95531 hydrobromide), DL-AP5, and NBQX were incubated with the slice for minimum of 10 minutes and included in puffer pipette along with the

agonist under test. All agonists and antagonists were obtained from Tocris (Bristol, UK).

Calcium imaging and calcium uncaging:

Astrocytic somatic calcium signals were quantified using 10 μ M Fluo4FF-AM or 10 μ M Fluo4-AM and neuronal calcium signals were quantified using 10 μ M Fluo4-AM (Molecular Probes, Eugene, OR). WT or MeCP2-null slices were prepared as above. After recovery at 35°C, slices were incubated in extracellular recording solution containing equal volumes of calcium indicator and 20% (w/v) Pluronic acid (Molecular Probes, Eugene, OR). These slices were maintained at 23°C for 25 minutes during which they were shielded from light and continuously bubbled with Carbogen. Slices were then transferred to the microscope stage and washed for 30 additional minutes with bubbled extracellular recording solution to allow for de-esterification of the calcium indicator. Live calcium signals were acquired using a Yokogawa CSU-X1 confocal spinning disc equipped with a Hamamatsu EM-CCD digital camera (Imagem-x2). The laser lines used were 488nm (OBIS Coherent, Santa Clara, CA) for calcium signals and 561nm (OBIS Coherent, Santa Clara, CA) for SR101 fluorescence. Laser power was set to <50%, which corresponded to a final output of 2.3mW for the 488nm line and 1.2mW for the 561nm line. Images were captured every 75msec beginning 2 seconds before drug application and continued until the calcium signal decayed. Micro-manager software (UCSF, San Francisco, CA) was used to acquire images and Image J (NIH, Bethesda, MD) and Microsoft Excel (Redmond, WA) were used for offline analysis. Throughout all of the experiments involving calcium imaging the laser and camera gains were held constant. Thus, it

became necessary to exclude those astrocytes, both mutant and wild type, that had high resting levels of calcium in order to prevent signal saturation. To quantitate calcium signals in astrocytes that qualified for analysis, the entire somatic region was selected as a region of interest (ROI). Then, for each ROI, the time dependent changes in signal intensity were quantitated as $\Delta F/F_0$ as follows. First, the average pixel intensity within each ROI was corrected for background fluorescence. To establish true background levels the average pixel intensity was determined using cells not incubated with the calcium indicator. Second, the background corrected basal fluorescence signal intensity (F_0) was determined on the basis of the average pixel intensity measured for the ROI during the two seconds prior to drug application. Third, the change in average fluorescence intensity for the ROI (ΔF) was determined by subtracting the average pixel intensity for the ROI by the background-subtracted basal fluorescence (F_0).

For calcium uncaging experiments, 4mM DMNP-EDTA (Molecular Probes, Eugene, OR) was loaded with 3.6mM CaCl_2 for 10 minutes in the dark. The astrocyte was then dialyzed with the loaded cage via the patch pipette along with 0.1mM Alexa Fluor 488 for at least 10 minutes. A shuttered, externally mounted fiber optic was used to trigger a 1 sec flash from an X-Cite 120 EXFO LED. Control astrocytes were dialyzed with an empty DMNP-EDTA cage and Alexa Fluor 488.

For certain experiments, the efficacy of the uncaging protocol was validated by use of a calcium indicating dye during the uncaging. For this purpose slices were incubated with 10 μM Fluo4FF and astrocytes were loaded with 4mM DMNP-EDTA caged calcium as previously described. Resting calcium levels were measured for ~ 2

sec using the 488nm laser line after which the calcium was uncaged using a 1 sec flash. At the time of uncaging, it was necessary to close the light path to the camera, limiting the calcium imaging and analysis to the time following termination of the flash.

Immunohistochemistry:

Coronal 80µm slices were cut from barrel cortex in ice cold 1xPBS, the cortex was removed and transferred to 4% paraformaldehyde (PFA) and fixed for 3 hours at 4°C. Slices were washed with 1xPBS containing 20mM glycine. Slices were then permeabilized with 1x PBS containing 0.2% triton x-100 for 15 minutes at 23°C. Slices were then blocked with 1x PBS containing 3% BSA and 5% normal goat serum for 30 minutes at 23°C followed with incubation in the respective primary antibody overnight at 4°C in the PBS-based blocking solution. After overnight incubation, the slices were washed and then incubated in secondary antibody for 2 hours at 23°C in the PBS-based blocking solution. Following exposure to the secondary antibody, slices were washed and then mounted using Prolong gold with DAPI. Primary antibodies used were: NeuN (1:200, Neuronal nuclei clone A60, MAB377, mouse monoclonal, Millipore, Darmstadt, Germany), GFAP (1:500, Glial Fibrillary Acidic Protein, Z0334, rabbit polyclonal, Dako, Santa Clara, CA), Par1 (1:100, Thrombin R, S-19, SC-8204, Goat polyclonal, Santa Cruz Biotechnology, Dallas, TX). Secondary antibodies used were: Alexa Fluor donkey anti goat-568 (1:500, A-11057), Alexa Fluor donkey anti rabbit-647 (1:500, A-31573), Alexa Fluor donkey anti mouse-488 (1:500, A-21202). All secondary antibodies were purchased from Thermo Fisher (Waltham, MA).

Western blotting:

Coronal 80µm slices were cut from barrel cortex in ice cold 1xPBS, the cortex was removed and immediately lysed in RIPA buffer (25mM Tris pH 7.6), 150mM NaCl, 1% NP40, 1% deoxycholate, 0.1%SDS, benzoate nuclease, protease inhibitor). Protein concentration was determined via BCA assay. 40µg of protein (boiled with loading dye at 70°C for 10 min) was run on a 4-12% bis tris gel with MOPS at 200volts for 1 hour. Gel was transferred to a nitrocellulose membrane using a methanol-based buffer for 1 hour at 100volts. Blot was blocked in 1x TBST with 3% BSA for 1 hour at 23°C and then incubated in primary antibody with 1x TBST and 1.5% BSA over night at 4°C. Following primary incubation, the blot was washed and then incubated in secondary antibody for 1 hour in 1xTBST with 3% BSA at 23°C. Blot was then washed before imaging on ODYSSEY. Primary antibodies used were: Par1 (1:5000, Thrombin R, S-19, SC-8204, Goat polyclonal, Santa Cruz Biotechnology, Dallas, TX), alpha-tubulin (1:10000, mouse monoclonal, DSHB #AA4.3, Iowa City, Iowa), MeCP2 (1:5000, rabbit monoclonal, cell signaling D4F3, 3456s, Danvers, MA). Secondary antibodies were conjugated to IR-fluorophore for imaging on Li-Cor Odyssey machine: goat anti mouse- IR680 (Thermo Fisher 35518, Waltham, MA), goat anti rabbit-IR680 (Thermo Fisher #33568, Waltham, MA) donkey anti goat- IR 800 (Li-Cor 925-32214, Lincoln, NE).

Chapter 3

Astrocyte-neuron signaling in wildtype cortex

To investigate signaling between wild type astrocyte-neuron pairs, cortical slices were made from mouse barrel cortex. This part of cortex was used for these experiments because there is precedence for astrocyte-mediated modulation of neuronal signaling (Benedetti et al., 2011; Schipke et al., 2008), astrocytes are plentiful and form distinct spatial domains (Mitterauer, 2010), and the local circuitry is well established (Stüttgen and Shwarz, 2017). Astrocytes were stimulated using either depolarization or agonist application and the effect on neuronal signaling was quantified in terms of electrophysiological recordings.

Depolarization-based astrocyte activation

Dual patch clamp recordings were performed on layer II/III pyramidal neurons and neighboring astrocytes in brain slices derived from the barrel cortex of postnatal (p10-12) wild type (WT) mice (fig. 1a,b). First, an astrocyte was selected on the basis of red fluorescence following incubation of the slice in 100nM sulforhodamine 101 (SR101; fig 1c). This dye is known to be preferentially internalized by astrocytes and a low concentration was used to limit potential off-target effects of SR101 on neuronal signaling (Hülsmann et al., 2017). Once the astrocyte was identified, a superficial proximal neuron was selected on the basis of

Figure 1- Dual patch clamp recording configuration.

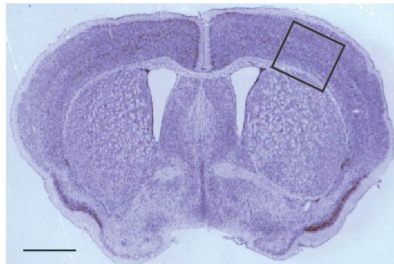
(a) Cross section of a p10 mouse brain through the barrel cortex region with an inset indicating the region from which astrocyte-neuron pairs were obtained for recording. Scale bar 1mm.

(b) Schematic representation of the inset area in A, noting the position of a neuron (black) and astrocyte (red) within the layers of the cortex.

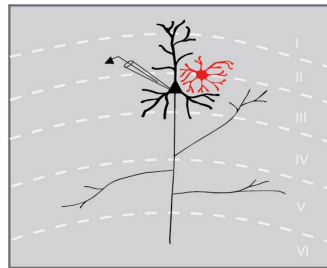
(c) Fluorescence counterpart to the image in d. showing the SR101 loaded astrocyte.

(d) DIC image of a cortical slice showing a typical recording configuration with the neuron recording on the left and astrocyte recording on the right.

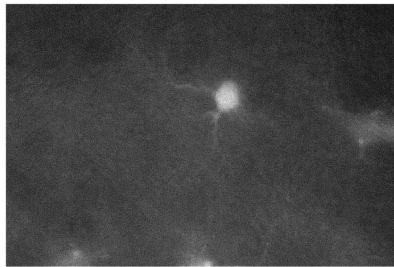
a.



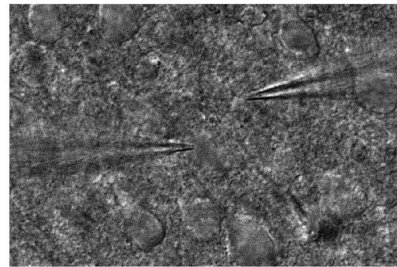
b.



c.



d.



soma morphology and size using DIC optics (fig 1d). Once the whole cell voltage clamp mode was established for both cells, the cellular identity was confirmed on the basis of input resistance, which is 4-fold higher for neurons ($143 \pm 24 \text{ m}\Omega$) compared to astrocytes ($35 \pm 12 \text{ m}\Omega$).

When held at -80 mV , both neurons and astrocytes could be further distinguished by spontaneous synaptic events (fig. 2a). Neuronal recordings were consistently associated with spontaneous events that represented a mixture of fast and slowly decaying excitatory synaptic currents. The synaptic events ranged in frequency from $99 \pm 39 \text{ events/min}$ to $537 \pm 147 \text{ events/min}$ with an amplitude range of $363 \pm 122 \text{ pA}$ to $4.6 \pm 2 \text{ pA}$, the latter representing the limits of our detection set by the noise level. The very largest events were generally the slowest decaying. Overall two populations of synaptic currents were typically identified, slower decaying with larger amplitude and faster decaying with smaller amplitude (figure 3.) By contrast, all astrocytes were quiescent, including during the time periods directly following the depolarization that was used to activate synaptic responses in the proximal neuron. Depolarization of the astrocytes using 20 consecutive 10 msec depolarizations led to a long lasting increase in the frequency of the synaptic currents in the proximal neuron, as indicated in the sample traces shown in figure 2 (fig. 2a). The increase in event frequency occurred within the first 5 sec following the onset of astrocyte depolarization, and persisted throughout the 60 sec post stimulation period (fig. 2b). Cumulative data from neuronal recordings indicated a significant increase in the frequency of synaptic currents following

Figure 2. Depolarization of astrocytes leads to increased frequency of synaptic currents in cortical neurons of WT mice.

(a) Representative traces of synaptic currents recorded from a WT neuron before (top) and after (bottom) administering 20, 10ms. +140mV steps to the astrocyte.

(b) The corresponding temporal sequence for WT synaptic current occurrence 60 sec prior to and 60 sec following astrocyte depolarization. The time of stimulation is indicated by the black bin.

(c) The cumulative results from 10 WT recordings showing the mean +/- pre and post stimulus event frequencies. $p=0.035$, $n=10$.

(d) The fold change for the individual recordings shown in C.

(e) Amplitude histograms for pooled recordings measured before (black) and after (gray) astrocyte stimulation, one statistical outlier is not graphically represented.

(f) The fold change in mean event amplitude for each recording and mean and S.D. are indicated.

All recordings were performed using symmetrical transmembrane chloride concentration

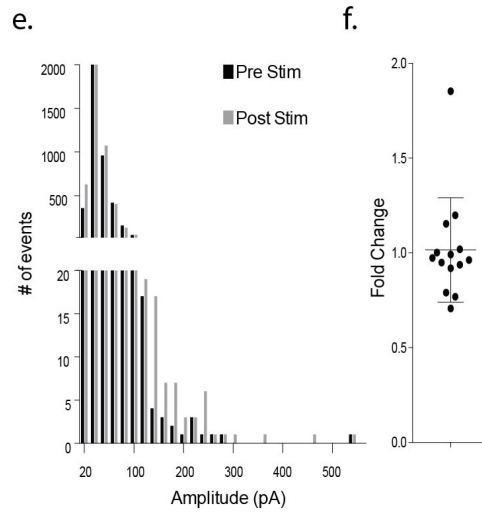
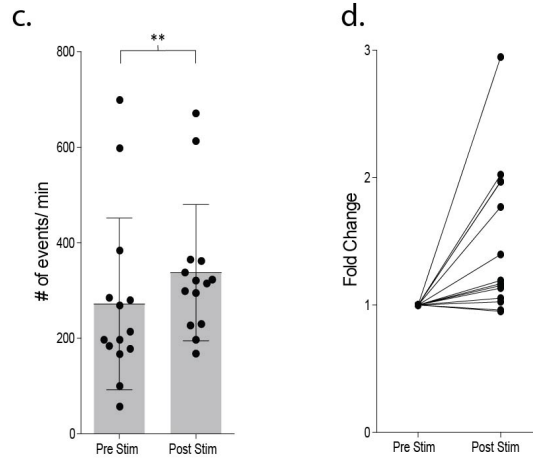
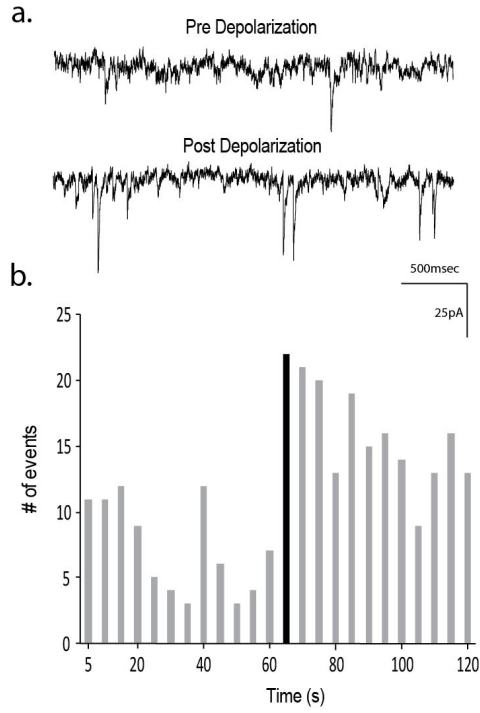


Figure 3. Distinct populations of synaptic currents.

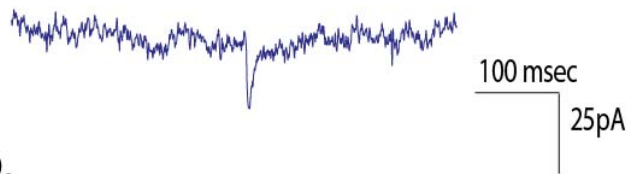
(a) Representative recording (500msec) of a synaptic current recorded from pyramidal neuron voltage clamped at -80mV.

Synaptic current amplitude= 24pA, rise time=1.88, τ = 4.78 (10%-90%)

(b) Representative recording (500msec) of a synaptic current recorded from pyramidal neuron voltage clamped at -80mV.

Synaptic current amplitude= 37pA, rise time=1.64, τ = 62.63 (10%-90%)

a.



b.



astrocyte depolarization (pre: 272 ± 180 events/min, post: 337 ± 143 events/min, $p=0.002$, $n=14$) (fig. 2c), which corresponded to an average 1.48 ± 0.58 fold increase in frequency (fig. 2d). The pooled amplitude distributions for pre- and post-stimulation were largely overlapping with the exception of the very largest events (fig. 2e). Expressed as fold change for individual experiments, there was no overall difference in the average amplitude before and after stimulation (pre: 31 ± 24 pA, post: 30 ± 27 pA; 1.02 ± 0.28 fold change; fig. 2f). However, there was a 2.5 fold increase in the number of post stimulation events with amplitudes >120 pA (pre: 22, post: 56; fig. 2e).

Given that astrocyte-mediated effects were seen in proximal neurons, I was interested to test how local these effects were. Triple patch recordings from wild type slices were used to determine whether the distance between the astrocyte and neuron influenced the frequency increase in synaptic currents following astrocyte stimulation. For this purpose, a single SR101 positive astrocyte was selected and two neurons were patch clamped. One neuron was proximal to the astrocyte (within one somal distance, $\leq 20\mu\text{m}$) and a second neuron was located at a variable distance from the astrocyte ($>20\mu\text{m}$). The effect of astrocyte depolarization on the frequency of synaptic currents was larger if the neuron was within $20\mu\text{m}$ (pre: 220 ± 108 events/min, post: 325 ± 182 events/min; fold change: 1.4 ± 0.1 , $n=5$) compared to distances up to $40\mu\text{m}$ away (pre: 174 ± 56 events/min, post: 211 ± 74 events/min; fold change: 1.2 ± 0.2 ; $n= 5$) though the effect of astrocyte depolarization was still felt at this distance (fig 4.).

Figure 4: Triple electrode recording between one astrocyte and two neurons at different distances from the astrocyte.

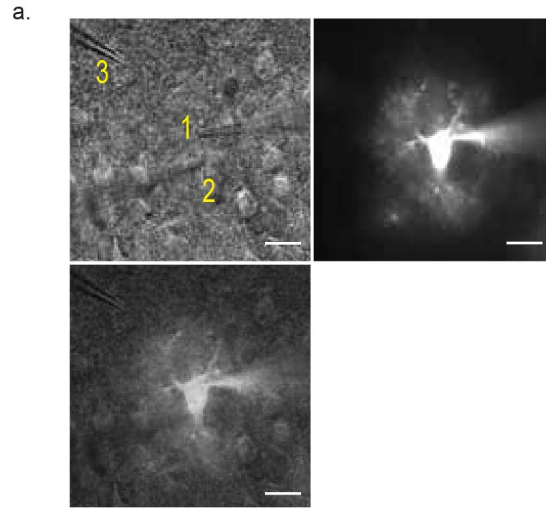
(a) Image of triple recording. Top left: DIC image of astrocyte (1), proximal neuron (2), and distal neuron (3). Top right: AlexaFluor 488 fill of astrocyte, exposure time was increased to capture astrocytic arbor. Bottom left: merge. Scale bar is 20 μ m.

(b) The triple recording from a) with the corresponding time line for synaptic current frequency from two neurons, one at 18 μ m (left) and one at 33 μ m (right) away from the astrocyte, with the time of astrocyte depolarization indicated by the black bin.

(c) A second representative triple recording as in (a), one neuron is 16 μ m (left) the other is 43 μ m (right) from the astrocyte.

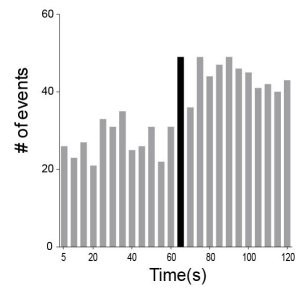
(d) Cumulative data from 5 triple recordings showing increased synaptic frequency upon astrocyte depolarization when the neuron is within 20 μ m.

(e) Corresponding fold changes for the recordings in (c).

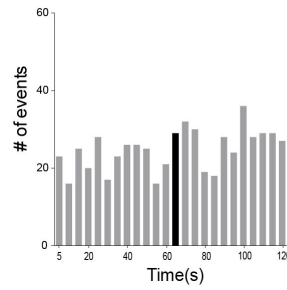


b. Triple recording 1

astrocyte 1 - neuron 2 (18 μ m)

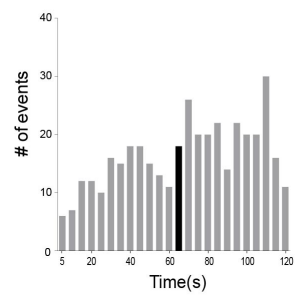


astrocyte 1 - neuron 3 (33 μ m)

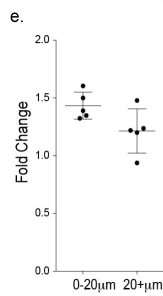
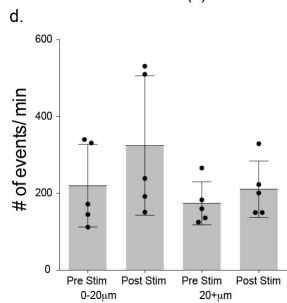
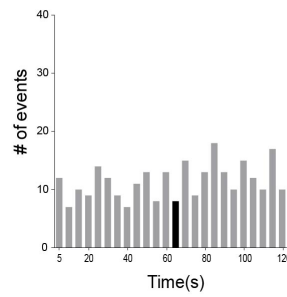


c. Triple recording 2

astrocyte-neuron 1 (16 μ m)



astrocyte-neuron 2 (43 μ m)



Agonist-based astrocyte activation

Given that astrocytes are not electrically excitable cells, I sought to use a more physiological means of activating the astrocytes. To this end, I exploited previous studies reporting that Protease Activated Receptor 1, Par1, is expressed preferentially in astrocytes over neurons (Junge et al., 2004). Par1 is a metabotropic receptor that activates Gq-coupled release of intracellular calcium and has a synthetic peptide agonist, TFLLR (Hollenberg et al., 1997), which I could deliver locally via puffer application (fig. 5). In our hands, immuno-labeling with a Par1 antibody (s-19) resulted in fluorescence that was associated exclusively with GFAP-positive astrocytes, with no visible labeling associated with NeuN-positive neurons (fig. 6). As an additional means to limit TFLLR activation to a single astrocyte, I selected SR101 positive astrocytes that were sufficiently separated from one another to be out of range for simultaneous puffer activation, and brought the puffer close to the astrocyte of interest to limit diffusion of the agonist. Like depolarization, the application of 500 μ M TFLLR ($EC_{50}=1.9 \mu$ M) to wild type astrocytes consistently resulted in an increase in synaptic event frequency in the proximal neuron recording, qualitatively similar to that seen with astrocyte depolarization (fig. 5a). Also like depolarization, the time course of synaptic current occurrence increased within five seconds of agonist application and persisted for the 60 sec post stimulus period (fig. 5b). Moreover, a significant increase in synaptic event frequency was recorded for astrocyte-neuron pairs tested (pre: 169 ± 81 events/min, post: 254 ± 116 events/min, $p=0.004$, $n=10$) (fig. 5c). When expressed as fold change, an average 1.59 ± 0.16 fold increase was observed (fig. 5d). Again, there was no change

Figure 5. TFLLR applied to astrocytes leads to increased frequency of synaptic currents in cortical neurons of WT mice.

(a) Representative traces of synaptic currents recorded from a WT neuron before (top) and after (bottom) following puffer application of 500 μ M TFLLR to the astrocyte.

(b) The corresponding time line for WT synaptic current frequency with the time of application indicated by the black bin.

(c) The cumulative results from 10 WT recordings showing the mean \pm pre and post application event frequencies. $p=0.004$, $n=10$ (d) The fold change for the individual recordings shown in C.

(e) Amplitude histograms for pooled recordings measured before (black) and after (gray) TFLLR application.

(f) The fold change in mean event amplitude for each recording and mean and S.D. are indicated.

All recordings were performed using symmetrical transmembrane chloride concentrations.

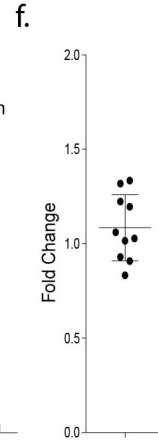
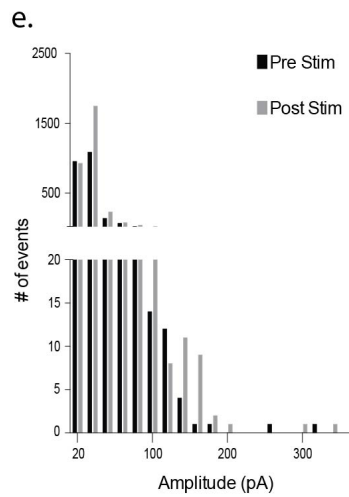
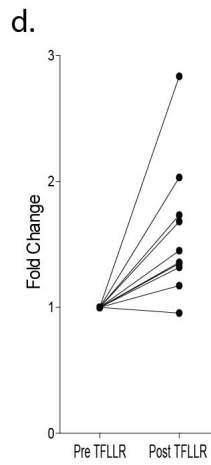
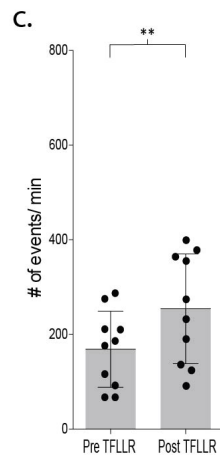
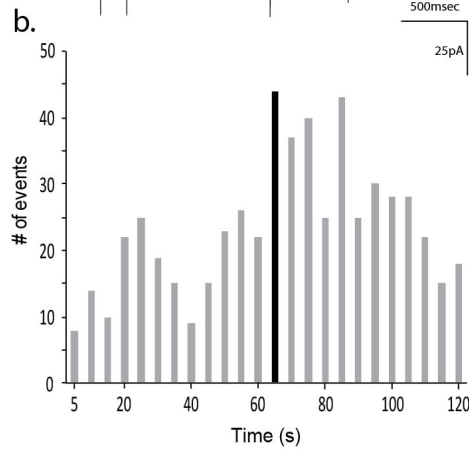
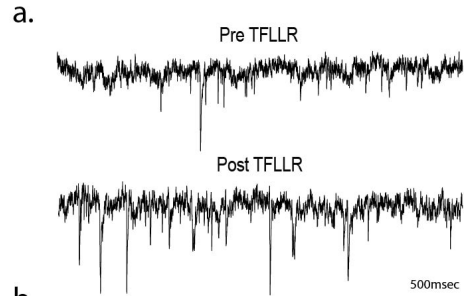


Figure 6: Immunohistochemical labeling of WT cortex for Par1.

(a) neuronal marker NeuN

(b) astrocytic marker glial fibrillary acidic protein (GFAP)

(c) protease activated receptor 1 (par1)

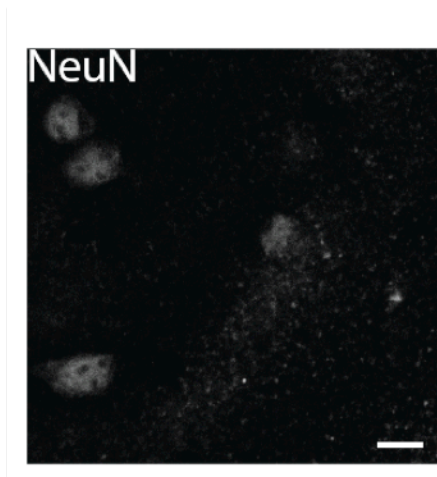
(d) nuclear marker DAPI

(e) merge of all four markers

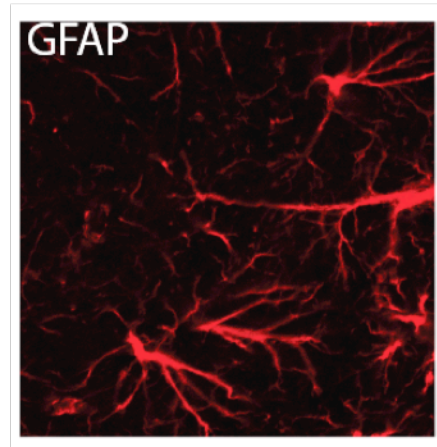
80µm thick Cortical slices

Scale bar is 20µm.

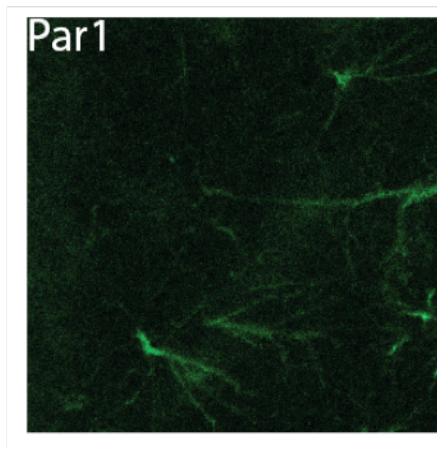
a.



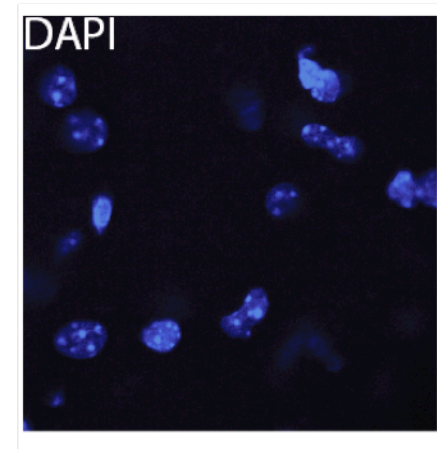
b.



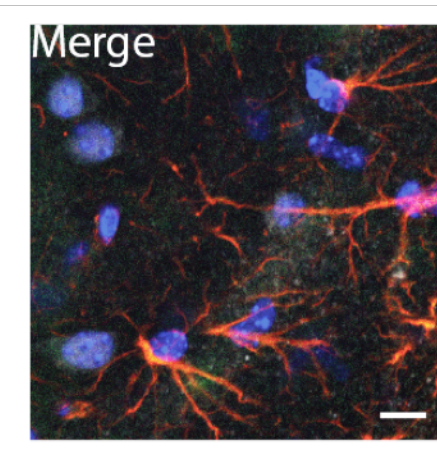
c.



d.



e.



in amplitude pre and post TFLLR application (fig. 5e, f), but there was a 1.9 fold increase in the number of events with amplitudes larger than 120 pA, as seen with depolarization of WT astrocytes (fig. 5e; pre: 15, post: 28).

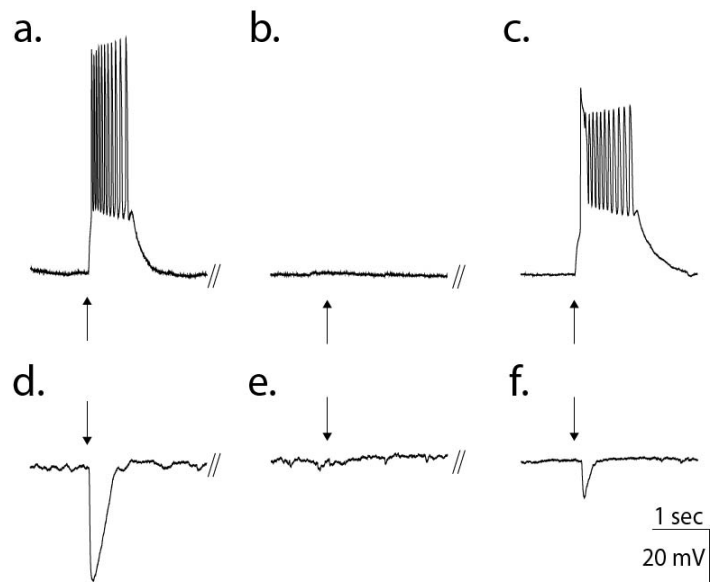
Astrocytes activate both glutamatergic and GABAergic signaling in neurons.

The principle neurotransmitters in the cortex are glutamate and GABA, which can be distinguished based on differences in the ion selectivities of the receptor channel types. In the data above, both receptor channels produced inward currents as a consequence of similar reversal potentials. Glutamatergic channels reversed near 0 mV owing to their nonselective cation permeability, while the anion selective GABA_A receptors reversed near 0mV due to the symmetrical chloride concentrations. Thus far, a symmetrical transmembrane chloride concentration was chosen for neuronal recordings, rendering GABA an excitatory transmitter. An excitatory action by GABA on neurons was confirmed by use of cell attached gramicidin perforated patch recordings. Gramicidin, being exclusively permeable to cations, allowed monitoring of synaptic currents through a low resistance pathway while leaving the natural transmembrane chloride gradient intact. Recordings from 16 neurons revealed that direct application of 50 μ M GABA depolarized the neuron to levels sufficient for action potential generation (fig. 8a), consistent with an excitatory profile at this developmental stage (p10-12). The depolarizing effect of GABA in these recordings was reversibly inhibited following treatment with 20 μ M gabazine (fig. 58 and 8). When held at 0mV under current clamp, 50 μ M GABA application led to a hyperpolarization (fig. 8), which was reversibly inhibited

Figure 8- Gramicidin perforated patch whole cell recordings confirm GABA as an excitatory transmitter at this developmental age.

(a-c) Current clamp traces from a cortical neuron with resting potential at -80 mV showing that direct application of 50 μ M GABA (arrow) resulted in a burst of action potentials that was reversibly blocked by 20 μ M gabazine (arrow).

(d-f) Current clamp traces from a cortical neuron with a membrane potential held at 0mV showing direct application of 50 μ M GABA (arrow) produced hyperpolarization that was reversibly blocked by 20 μ M gabazine (arrow).



following treatment with 20 μ M gabazine (fig. 8e and f). Indicating that the reversal potential for GABA-mediated current was <0mv.

I then utilized the differences in ion selectivity between GABA_A and glutamate receptors to simultaneously monitor the respective contributions of the individual signaling pathways by lowering the internal chloride concentration. This non-physiological asymmetry shifted the GABA_A receptor reversal potential from ~0mV to -70mV. Holding the membrane potential of the neuron between the reversal potentials for the different receptor types (-35mV) created inward and outward currents (fig. 9a). Assignment of the outward currents to GABA_A and inward currents to glutamate receptors was confirmed with pharmacology. Under basal conditions, 86% of outward events were inhibited by gabazine (pre-gabazine: 18 \pm 8 events/min, post-gabazine: 2.6 \pm 1.3 events/min; p= 0.008, n=8) with no significant contributions by inward currents (pre-gabazine: 101 \pm 46 events/min, post-gabazine: 85 \pm 35; p=0.117, n=8) (fig. 9b). Inhibition of NMDA and AMPA glutamate receptors with AP5/NBQX reduced the inward current frequency by 66% (pre-AP5/NBQX: 104 \pm 45 events/min, post-AP5/NBQX: 35 \pm 17; p=0.0005, n=12), with no significant contributions from the outward current class (pre-AP5/NBQX: 38 \pm 13, post-AP5/NBQX: 41 \pm 18, p=0.386, n=12) (fig 9c).

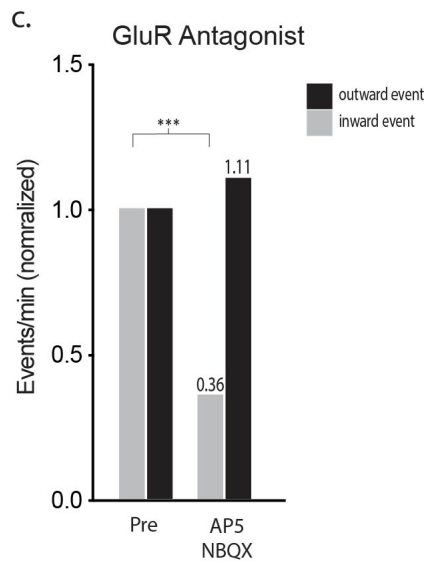
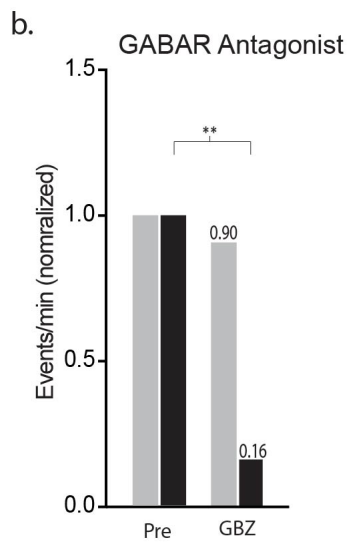
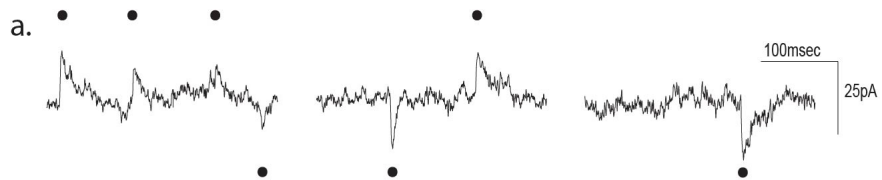
Figure 9. Bidirectional currents reveal the individual basal contributions by GABAergic and glutamatergic signaling

(a) Low chloride internal solution produces inward and outward currents in cortical neurons when held at -35 mV. Three 300 msec representative traces are shown.

(b) Event frequency normalized to the first 60 sec pretreatment period. Slices were incubated in 20 μ M gabazine for 10 minutes and the frequency of outward and inward events was quantified (outward: $p=0.008$, inward: $p=0.117$, $n=8$).

(c) The same as B only GluR receptor inhibitors AP5 (50 μ M) and NBQX (5 μ M) tested (inward: $p=0.0005$, outward: $p=0.386$, $n=12$ recordings).

All recordings were performed using low intracellular chloride concentrations while neurons were held at -35mV.



Using the directional indicators, we re-tested contributions of each receptor class to the overall TFFLR stimulated increase in current frequency. In WT recordings, TFFLR application increased the frequency of inward currents by an average 1.70 ± 0.13 fold (pre- TFFLR: 156 ± 68 events/min, post- TFFLR: 259 ± 117 events/min, $p= 0.001$, $n=11$) (fig.10 a, b). Outward currents were increased 1.6 ± 0.2 fold in 9 out of 11 recordings (pre-TFFLR: 50 ± 23 events/min, post-TFFLR: 79 ± 44 events/min, $p=0.005$, $n=11$; fig. 10 c, d). These data suggest that astrocyte activation modulates both glutamate-mediated and GABA-mediated neuronal signaling.

Figure 10. The relative contributions of inward and outward currents to astrocyte-mediated increases in neuronal signaling are quantified.

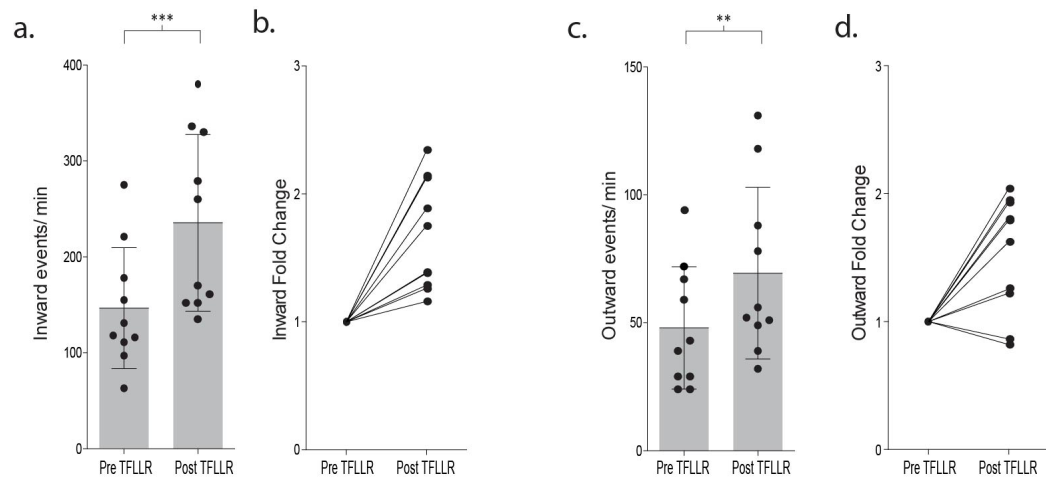
(a) The frequency of inward events is quantified before and after 500 μ M TFLLR application, grey box indicates mean \pm SD ($p= 0.001$, $n=11$).

(b) The corresponding fold-change for the individual recordings.

(c) The frequency of outward events quantified before and after 500 μ M TFLLR application, grey box indicates mean \pm SD ($p=0.005$, $n=11$).

(d) The fold change for the individual recordings. All recordings were performed using low intracellular chloride concentrations while neurons were held at -35mV.

All events are normalized to the pre-stimulus 60 sec recording. Statistical tests were run on frequency counts before fold change was calculated and normalized.



Mechanism of gliotransmission

In order to build a model for how astrocytes modulate neuronal signaling, experiments were carried out to elucidate mechanisms of gliotransmission. To first test for direct chemical transmission from the astrocyte onto the neuron, I tested for time-locked, synchronized responses in the neuron upon depolarization of the astrocyte that are tetrodotoxin (TTX) sensitive, second, to test for the recruitment of neuronal inputs in driving agonist-based astrocyte-mediated effects TTX treatment was repeated with TFLLR application, third, I stimulated astrocytes in the presence of different antagonists to establish if blocking certain receptors abolished the astrocyte-mediated modulation in order to indirectly identify gliotransmitter(s), and, lastly, I tested for the involvement of vesicles and/or anion-permeant channels in the modulation of neuronal signaling.

A common method for characterizing the response properties of synaptically coupled cells is to test for time-locked events in response to astrocyte depolarization. By referencing the frequency of events that are within a short timeframe of astrocyte depolarization, one can determine the relevance of synaptic currents to the astrocyte stimulation. To accomplish this quantification, astrocytes were stimulated with one +140mV step at 1hz for 100 seconds while the synaptic events in a proximal neuron were analyzed within a 200msec window before and after the voltage step. Low frequency stimulation was essential in preventing the large-scale astrocyte-mediated modulation of neuronal signaling found with stronger stimuli (figure 2). After pooling 15 neurons, the appearance of synaptic currents in a proximal neuron increased 1.7 fold 40msec after astrocyte

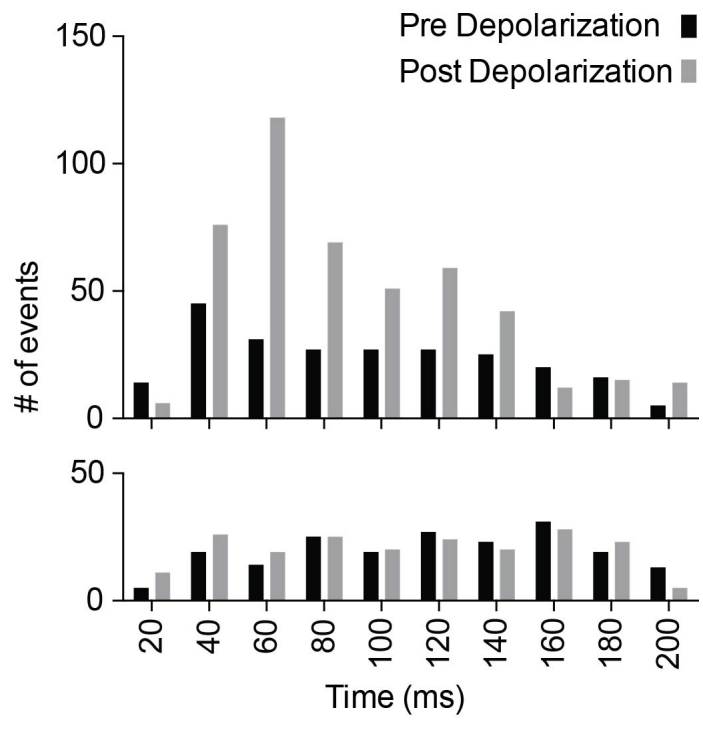
depolarization, was highest at 60msec after astrocyte depolarization (3.8 fold), and decreased to normal levels by 160 msec (figure 11 upper). The synchrony in the appearance of the synaptic currents suggests they are associated with the astrocyte depolarization, though the delay in the onset is evidence for gliotransmission being a slow process. The delay may also be explained by the recruitment of multiple presynaptic neurons to drive release onto the voltage clamped neuron, as these peaks were not seen in the presence of 1 μ M TTX which inhibited all stimulus driven signaling (fig. 8 lower). Furthermore, astrocytes have been reported to lack active zones (Bezzi et al., 2004; Jourdain et al 2007); meaning gliotransmitter release is not an organized, directional process, further implicating the recruitment of neighboring neurons.

Figure 11. Distribution of time-locked neuronal events in response to astrocyte depolarization.

(Upper) A frequency histogram showing the timing of synaptic events recorded over a 200ms period prior to (black) and after (grey) the astrocyte depolarization (a single 20ms voltage step to +40 mV). Event number is based on 20ms bins. Data represents accumulated events from 100 trials, each separated by 1s (n=15 neurons).

(Lower) A frequency histogram generated under similar conditions but acquired in the presence of 1 μ M TTX (n=6 neurons).

Recordings were taken at -100 mV and with a symmetrical chloride internal solution



To determine if the effect of agonist-based astrocyte activation on the frequency of neuronal events requires the recruitment of neighboring neurons, I repeated the blockade of neuronal action potentials using the selective sodium channel blocker TTX. TTX was not found to have an effect on astrocyte activation given that there were no astrocyte sodium currents during voltage steps (data not shown), and that the agonist-based stimulation of the astrocyte does not require action potential generation. When astrocytes were activated using TFLLR in the presence of 1 μ M TTX, the increase in synaptic current frequency was blocked in 4/5 recordings (pre: 231 \pm 142 events/min, post: 297 \pm 178 events/min; p= 0.125, n=5; Figure 12a and b). These data show that in the majority of astrocyte-neuron pairs tested, voltage-gated sodium channels are required for astrocyte-mediated modulation of neuronal signaling. Being that astrocytes do not express voltage-gated sodium channels in p10-p12 barrel cortex and that TTX blocked time-locked events in response to astrocyte depolarization, these data suggest that astrocytes are exciting neighboring neurons to release neurotransmitter onto the voltage-clamped post-synaptic neuron.

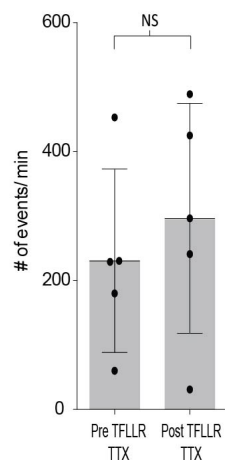
Figure 12. Blocking voltage-gated sodium channels with TTX prevented the TFLLR-mediated increase in the frequency of synaptic currents.

(a) The frequency of synaptic currents was quantified before and after 500 μ M TFLLR application in the presence of 1 μ M TTX, grey box indicates mean \pm SD (pre: 231 \pm 142 events/min, post: 297 \pm 178 events/min; p= 0.125, n=5)

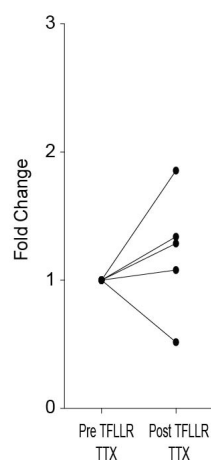
(b) The corresponding fold-change for the individual recordings in a.

- Symmetrical chloride internal was used, neuron voltage clamped at -80mV

a.



b.



To test whether direct, non-vesicular chemical transmission between the astrocyte and a proximal neuron could be identified, bafilomycin A1 (baf) was used. Baf is an inhibitor of the vacuolar type H⁺-ATPase (V-ATPase), which depletes the contents of synaptic vesicles by preventing their acidification. By blocking all vesicle-based signaling in the slice with baf treatment, any remaining astrocyte-mediated effect would implicate a non-canonical form of communication between the astrocyte and neuron. Slices were incubated in 2 μM baf for 1 hour at 23°C and the effect on the frequency of basal and astrocyte-evoked synaptic currents was quantified. The potent reduction in the basal frequency of synaptic currents confirmed that baf was successful in depleting vesicles (the average number of events per minute from figure 5 without baf treatment: 169 ± 81 , n= 10; the average number of events per minute after baf treatment: 14 ± 3 , n=6; p=0.0002; Figure 13a). Baf treatment also successfully blocked the TFLLR-mediated increase in neuronal signaling (pre: 14 ± 3 events/min, post: 11 ± 6 events/min; p= 0.31, n=6; Figure 13b and c). These data indicate that astrocyte-mediated effects require baf-sensitive vesicle, and, taken with the TTX data, the increase in frequency of synaptic currents after astrocyte activation is the result of astrocytes driving neuron-to-neuron signaling.

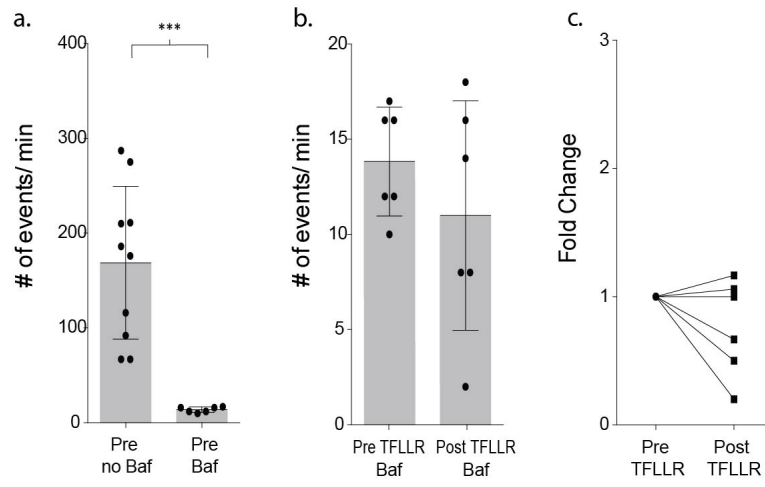
Figure 13. Bafilomycin treatment successfully depleted vesicular contents and blocked the TFLLR-mediated increase in the frequency of synaptic currents.

(a) The basal frequency of events pre and post bafilomycin (baf) treatment (2 μ M). The number of events/min pre baf is a representative amount taken from figure 5 (169 \pm 81 events/min, n= 10). Slices were incubated in baf for one hour before use, baf treatment significantly reduced the number of synaptic currents (14 \pm 3 events/min).

(b) Baf treatment blocked the TFLLR-mediated increase in synaptic current frequency (pre: 14 \pm 3 events/min, post: 11 \pm 6 events/min; p= 0.31, n=6)

(c) The corresponding fold-change for the individual recordings in b.

- Symmetrical chloride internal was used, neurons voltage clamped at -80mV.



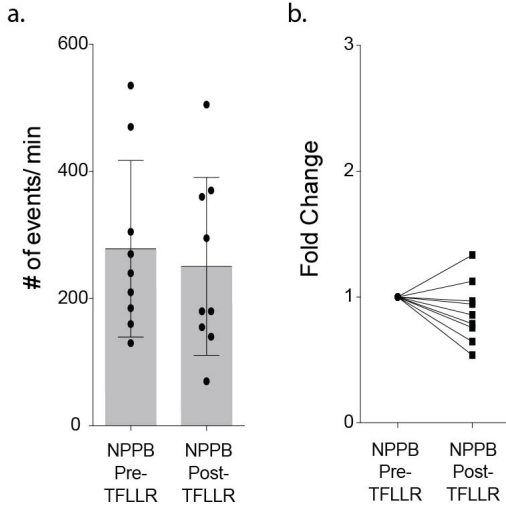
Recently, the astrocytic release of gliotransmitters has been reported to involve permeation through the bestrophin1 (best1) anion channel. Best1 is selectively expressed in astrocytes and has been found to be permeant to both glutamate and GABA in a calcium-dependent manner (Lee et al., 2010). To test whether best1 is involved in the aforementioned astrocyte-mediated effects, slices were treated with a blocker of calcium-activated chloride channels, 5-Nitro-2-(3-phenylpropylamino) benzoic acid, NPPB (100 μ M), and the TFLLR-mediated increase in neuronal signaling was quantified. Interestingly, treatment with NPPB blocked the astrocyte-mediated increase in the frequency of neuronal events (pre: 278 \pm 139 events/min, post: 251 \pm 140 events/min; $p= 0.152$, $n=9$; Figure 14). Unfortunately, NPPB is commonly used to block all calcium-activated chloride channels and therefore these data only suggest that Best1, and other calcium-activated chloride channels, participate in driving the astrocyte-mediated modulation of neuronal signaling.

Figure 14. Blocking calcium-activated chloride channels with 100 μ M NPPB eliminated the TFLLR-mediated increase in the frequency of synaptic currents.

(a) The frequency of synaptic currents was quantified before and after 500 μ M TFLLR application in the presence of 100 μ M NPPB, grey box indicates mean \pm SD (pre: 278 \pm 139 events/min, post: 251 \pm 140 events/min; p= 0.152, n=9)

(b) The corresponding fold-change for the individual recordings in a.

- Symmetrical chloride internal was used, neurons voltage clamped at -80mV.



In an attempt to determine whether the astrocyte was releasing either GABA or glutamate as the initiator of neuronal signaling, I applied the low-chloride internal solution to pharmacology-based experiments. The ability to separately block the inward and outward currents provided a means for testing whether release of either GABA or glutamate from astrocytes are responsible for initiation of neuronal signaling. For example, after blocking outward currents with gabazine, should TFFLR still activate inward currents, GABA could be effectively ruled out as the activator. Indeed, in the presence of gabazine only the outward currents were blocked (pre-TFFLR: 9 ± 2 events/min, post-TFFLR: 9 ± 3 events/min, $p = 0.732$, $n=14$) (figure 15a) leaving an increase in frequency of inward events intact (pre-TFFLR: 169 ± 58 events/min, post-TFFLR: 195 ± 74 events/min, $p = 0.004$, $n=14$) (figure 15a). Next, GluR blockers were tested for effects on both inward and outward currents. Consistent with the effects on basal current frequency (figure 9), AP5/NBQX provided only a partial block of inward currents, with no effect on outward currents (figure 15b). The application of TFFLR in the presence of AP5/NBQX failed to provide statistically significant increases in either inward (pre-TFFLR: 89 ± 46 events/min, post-TFFLR: 96 ± 61 events/min, $p = 0.61$, $n=15$) or outward currents (pre-TFFLR: 40 ± 25 events/min, post-TFFLR: 52 ± 39 events/min, $p = 0.124$, $n=15$) (figure 15b). To determine if ATP is released by astrocytes to initiate neuronal signaling, the P2 purinergic receptor antagonist PPADS was used. PPADS treatment blocked the TFFLR-mediated increase in inward currents (pre-TFFLR: 115 ± 35 events/min, post-TFFLR: 120 ± 25 events/min, $p = 0.392$, $n=12$), however the increase in frequency of outward currents persisted (pre-

TFFLR: 27 ± 8 events/min, post-TFFLR: 31 ± 11 events/min, $p= 0.029$, $n=12$) (figure 15c). Given that no statistically significant increase in either inward or outward current frequency was observed in the presence of glutamate receptor blockers, the results are consistent with glutamate (or d-serine) representing the transmitter. However, the persistence of many outward current responses in the presence of AP5/NBQX could reflect incomplete block or, possibly, contributions by an additional transmitter to the inward current class.

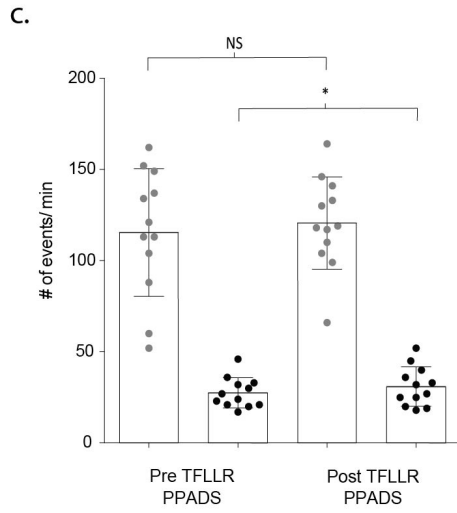
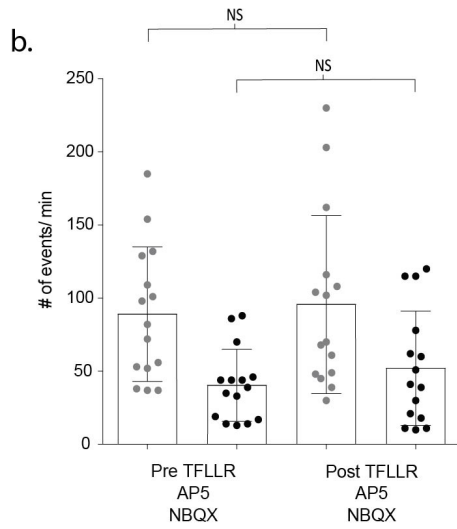
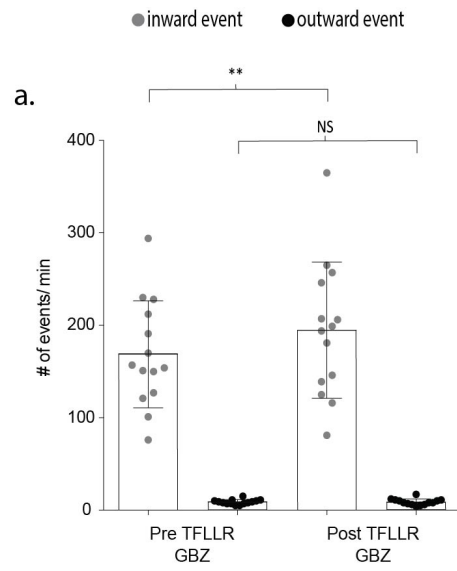
Figure 15. Testing the role of GABA, glutamate, d-serine, and ATP as transmitters for astrocytic activation of neuronal signaling.

(a) The frequency of inward and outward events before and after 500 μ M TFLLR application in the presence of 20 μ M GBZ (inward currents: $p= 0.004$, $n=14$; outward currents: $p=0.732$, $n=14$).

(b) The frequency of inward and outward events before and after 500 μ M TFLLR application in the presence of 50 μ M AP5 and 5 μ M NBQX (inward currents: $p= 0.61$, $n=15$; outward currents: $p=0.124$, $n=15$).

(c) The frequency of inward and outward events before and after 500 μ M TFLLR application in the presence of 100 μ M PPADS (inward currents: $p= 0.392$, $n=12$; outward currents: $p=0.029$, $n=12$).

- Box and bars indicate the mean \pm SD respectively.
- Low chloride internal was used, neurons voltage clamped at -35mV.



Chapter 4

Astrocyte-neuron signaling in Rett cortex

The purpose for the following experiments was to elucidate the cellular interactions between astrocytes and neurons in a mouse model of RTT. Previous work from the Mandel lab had identified an astrocytic component in the disease. Co-culture experiments had found that MeCP2-deficient astrocytes had aberrant intracellular processes and failed to support proper neuronal development (Ballas et al., 2009; Turovsky et al., 2015; Yasui et al., 2017; Delépine et al., 2016; Williams et al., 2014; Okabe et al., 2012; Garg et al., 2015). Importantly for this dissertation, when MeCP2 was restored specifically in astrocytes by a conditional *Cre* approach, in otherwise *Mecp2* null mice (Lioy et al., 2011), several hallmark behavioral deficits, including premature lethality and respiration abnormalities, were ameliorated significantly, leading to the idea that astrocytes affect RTT disease progression.

The previous chapter established that astrocytes are capable of modulating neuronal signaling. The following experiments utilized electrophysiology as a means to uncover differences in the intercellular interaction between astrocytes and neurons in two mouse models of RTT, a global null male mouse that is the most severe form of RTT and a heterozygous female mouse that is the most accurate representation of human RTT.

Astrocyte-mediated modulation of neuronal signaling is absent in MeCP2-null cortex

In order to test how astrocyte-mediated modulation of neuronal signaling is affected in RTT paired patch clamp recordings were repeated using cortical slices obtained from male mice that were germline null for MeCP2. Representative traces illustrate the absence of depolarization-activated changes in synaptic current frequency following astrocyte stimulation (figure 16a). The corresponding time course for event frequency also failed to show a significant increase in astrocyte-mediated synaptic current frequency, distinguishing it from wild type recordings (figure 16b). This absence of astrocyte-mediated effects was reflected for all MeCP2 deficient pairs tested (pre: 260 ± 140 events/min, post: 267 ± 162 events/min, $p=0.57$, $n=10$) (figure 16c) as in the fold changes (1.01 ± 0.04 fold; figure 16d). Additionally, in the mutant recordings there were no effects of depolarization on either the overall amplitude of synaptic currents (figure 16e) or on the class of events >120 pA, representing the largest amplitude class (figure 16e, f).

TFLLR was next tested for its ability to activate neuronal signaling in slices from MeCP2 null male mice (figure 16g-l). Representative traces prior to and following TFLLR application demonstrated a failure to observe an increase in event frequency (figure 16g). As with depolarization, the time course measurements for synaptic events from that recording showed no stimulus associated increase in frequency (figure 16h). Additionally, the cumulative data for all astrocyte-neuron pairs showed no significant increase in event frequency following agonist application

Figure 16. Astrocyte-mediated modulation of neuronal signaling is absent in MeCP2-deficient animal.

(a) Representative traces (3 sec) of synaptic currents recorded from a KO neuron before (top) and after (bottom) administering 20, 10ms. +140mV steps to the KO astrocyte.

(b) The corresponding temporal sequence for KO synaptic current occurrence 60 sec prior to and 60 sec following astrocyte depolarization. The time of stimulation is indicated by the black bin.

(c) The cumulative results from 10 KO recordings showing the mean +/- pre and post stimulus event frequencies. $p = 0.57$, $n = 10$

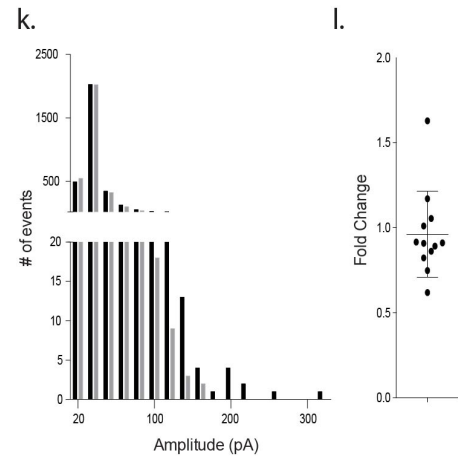
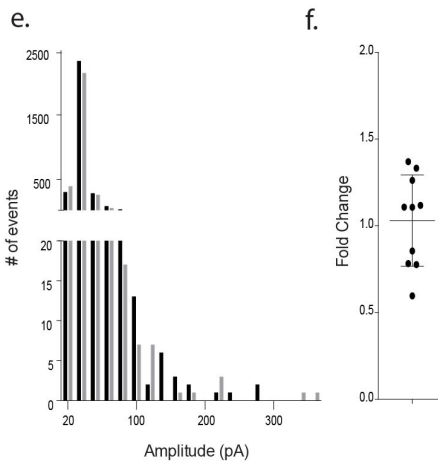
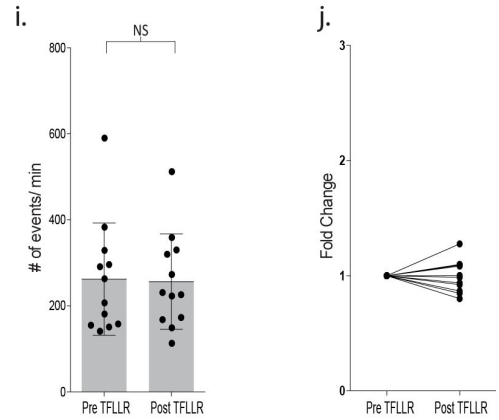
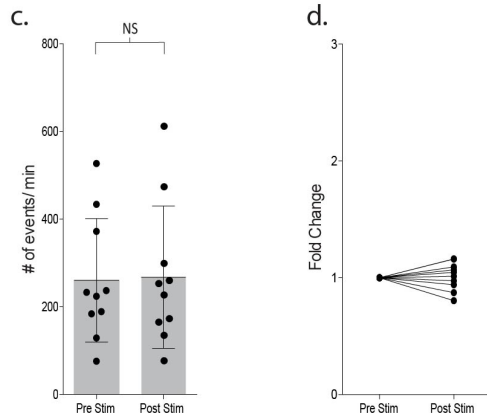
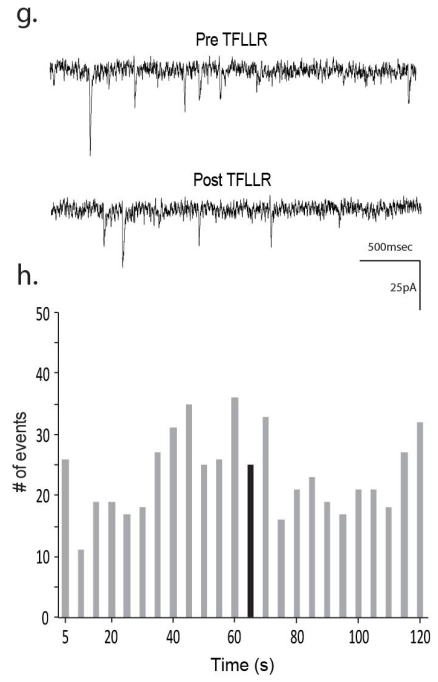
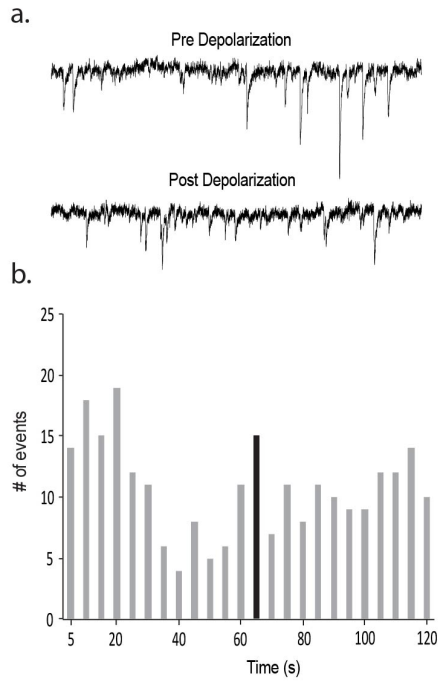
(d) The fold change for the individual recordings shown in C.

(e) Amplitude histograms for pooled recordings measured before (black) and after (gray) astrocyte stimulation, one statistical outlier is not graphically represented.

(f) The fold change in mean event amplitude for each recording and mean and S.D. are indicated

(g-l) Complementary sample recordings, time course and cumulative findings obtained from MeCP2 null male mice after TFLLR application. $p = 0.68$, $n = 12$.

All recordings were performed using symmetrical transmembrane chloride concentrations.



(pre: 262 ± 131 events/min, post: 256 ± 111 events/min, $p = 0.68$, $n = 12$) (figure 16). When expressed as fold change, only 1 out of the 12 pairs tested responded positively. Overall, there was no significant increase in event frequency as reflected in the 1.00 ± 0.04 fold change (figure 16j). Finally, no change in amplitude was observed for the pooled events (figure 16k) or in the fold change for individual recordings (figure 16l).

Given the lack of astrocyte-mediated effects with the agonist-based activation of the astrocyte, I sought to ensure that this defect was not due to differential expression of par1 in the MeCP2 null cortex. First, I repeated the immuno-labeling done in WT cortex (figure 6), staining MeCP2-null barrel cortex slices with the par1 antibody (s-19) also resulted in fluorescence that was associated exclusively with GFAP-positive astrocytes with no visible labeling associated with NeuN-positive neurons (figure 17). In order to compare levels of the par1 protein between WT and MeCP2-null cortex, cortical lysates were blotted and stained for MeCP2 and par1 epitopes. After normalizing to alpha tubulin as a loading control, no difference in the amount of par1 was found between WT cortex and MeCP2-null cortex (WT normalized par1 = 0.92 AU, KO normalized par1 = 1.09 AU) (figure 18).

Figure 17. Immunohistochemical labeling of MeCP2 null cortex for Par1.

(a) neuronal marker NeuN

(b) astrocytic marker glial fibrillary acidic protein (GFAP)

(c) protease activated receptor 1 (par1)

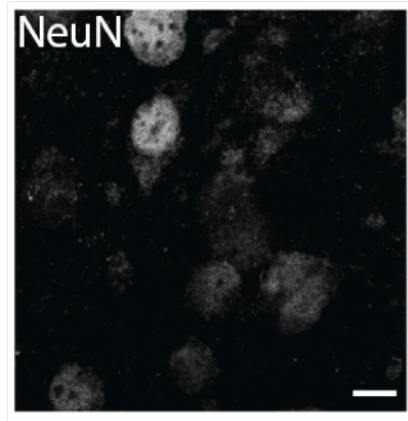
(d) nuclear marker DAPI

(e) merge of all four markers

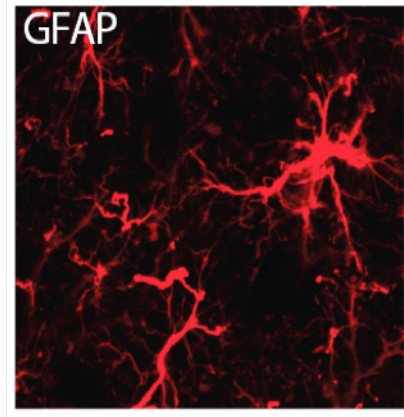
80 μ m thick Cortical slices

Scale bar is 20 μ m.

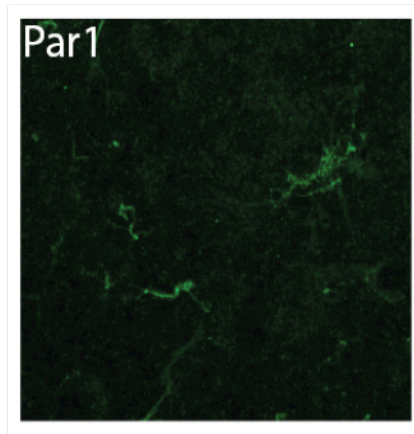
a.



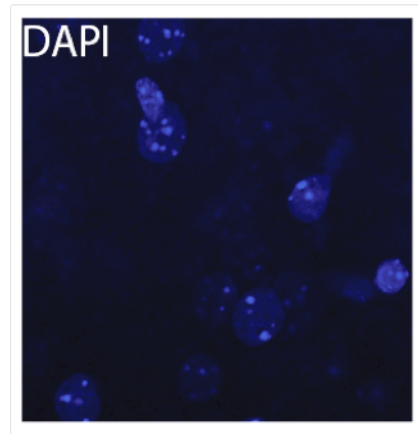
b.



c.



d.



e.

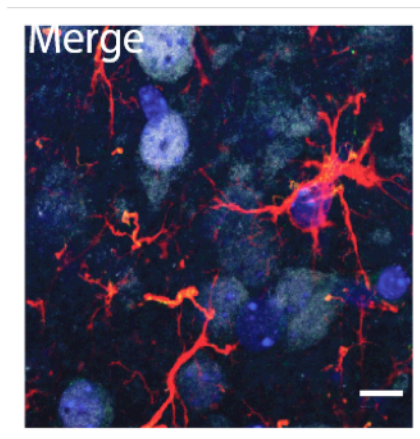
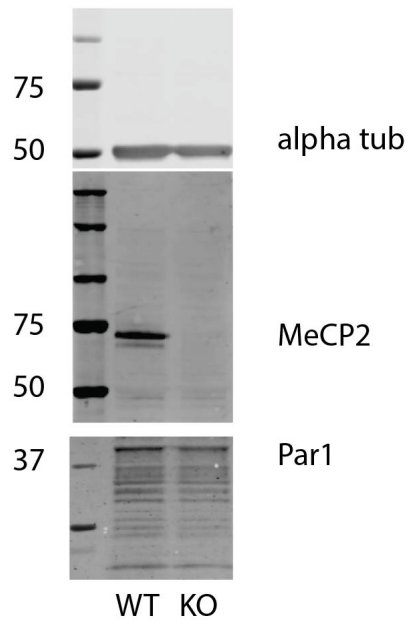


Figure 18. Western blot showing astrocyte specific Par1 immunoreactivity in lysates from cortex.

Equal amounts of protein (40µg) from WT and MeCP2 null cortical lysates were blotted and stained for MeCP2 and Par1 epitopes. Alpha tubulin was a loading control. Alpha tubulin and Par1 staining was performed on the same blot, but the blot was cut for simultaneous staining. MeCP2 staining was from the same lysate as that used for alpha tub and Par 1, but the lysate was run on a different gel for the blot.



To examine more carefully for changes in either GABA or glutamate mediated event frequency for MeCP2-null recordings they were parsed into inward and outward currents by use of lowered internal chloride. Recordings from MeCP2 deficient slices showed no significant increases in either outward or inward current frequency in response to TFFLR. The frequency of inward events corresponded to a 0.91 fold change (pre: 83 ± 33 events/min, post: 77 ± 32 events/min, $p= 0.25$, $n=6$) (figure 19a and b) and the frequency of outward events corresponded to a 0.83 fold change (pre: 25 ± 11 events/min, post: 20 ± 9 events/min, $p= 0.09$, $n=6$) following agonist application (figure 19c and d). This confirms the findings from symmetrical chloride conditions showing no stimulus driven increase in synaptic event frequency. Furthermore, analysis of the basal frequency revealed a similar 3:1 ratio for inward to outward currents in MeCP2 deficient (inward: 83 ± 33 events/min, outward: 25 ± 11 events/min) and wild type (inward: 156 ± 68 events/min, outward: 50 ± 23 events/min) recordings (figure 10a-d and figure 19a-d).

Figure 19. The relative contributions of outward and inward currents as a result of null astrocyte activation.

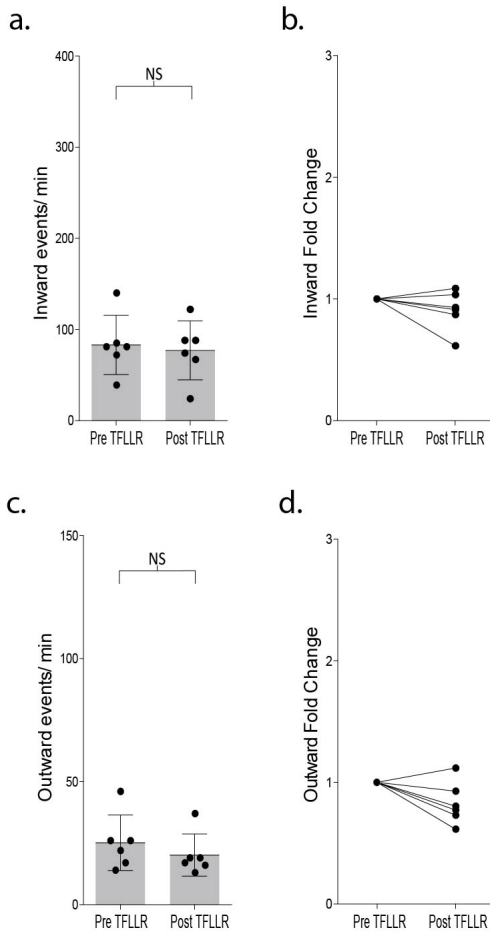
(a) The frequency of inward events is quantified before and after 500 μ M TFLLR application, grey box indicates mean \pm SD ($p= 0.25$, $n=6$).

(b) The fold-change for the individual recordings in a. are shown.

(c) The frequency of outward events for the same pairs in a and b is quantified before and after 500 μ M TFLLR application, grey box indicates mean \pm SD ($p= 0.09$, $n=6$).

(d) The fold change for the individual recordings in o. are shown.

Low intracellular chloride concentrations were used while neurons were held at -35mV



The Expression of MeCP2 in astrocytes, not neurons, is required for the astrocyte-mediated modulation of neuronal signaling.

The previous measurements compared astrocyte-mediated effects between WT and MeCP2 global null male mice. In these mice, all cells lacked MeCP2 expression. To test directly whether the defective signaling resided in the astrocyte, neuron, or both cell types, we turned to heterozygous mutant female mice that are mosaic for loss of MeCP2 due to dosage compensation. Further, these mice contain a knock in of GFP into the endogenous *Mecp2* gene, such that in the heterozygous condition, only the WT cells are fluorescent. Thus, MeCP2-GFP was expressed in ~50% of all neurons and astrocytes, whereas the remaining 50% of the cells expressed a truncated, nonfunctional MeCP2 protein (Lyst et al., 2013). These MeCP2-GFP heterozygous mice provided the opportunity to record from all pairwise combinations of WT (GFP positive) and MeCP2-null (GFP negative) astrocytes and neurons.

To ensure astrocyte-mediated neuronal signaling remained intact in this mosaic line, we first recorded from a MeCP2-GFP positive astrocyte/ neuron pair (figure 20a). Depolarization of the MeCP2 positive astrocyte/neuron pair increased the frequency of synaptic events by 1.60 ± 0.23 fold (Pre: 150 ± 38 events/min, Post: 233 ± 77 events/min, $p=0.04$, $n=6$) (figure 20b, c) recapitulating the findings from WT male mice. When MeCP2-negative astrocyte/neuron pairs were tested, there was no observed increase in the frequency of neuronal synaptic currents (Pre: 147 ± 42 events/min, Post: 155 ± 38 events/min, $p=0.24$, $n=7$) (figure 20d- f)

Figure 20- Defective signaling in astrocyte-neuron pairs results from the MeCP2 null astrocytes and not the neurons.

(a) Images shown the DIC image (left), SR101+ astrocyte (middle) and GFP+ astrocyte and GFP+ neuron (right).

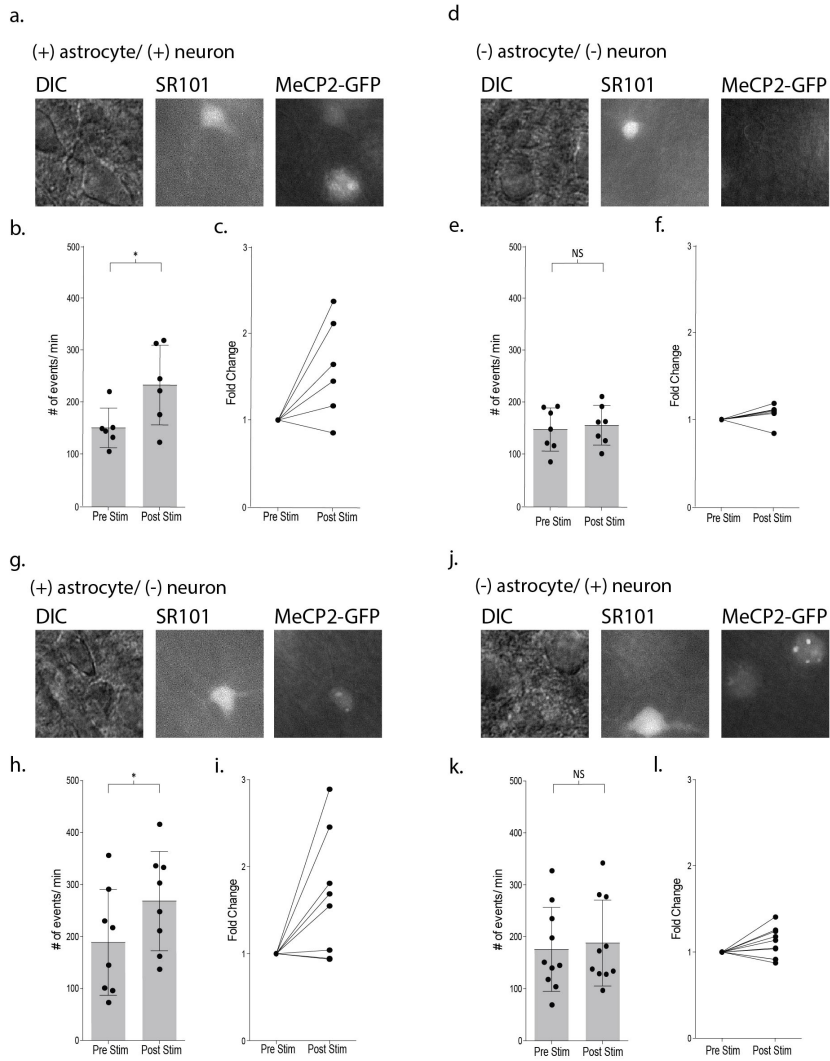
(b) The mean \pm SD event frequency for each neuron recording prior to depolarization and following depolarization. $p=0.04$, $n=6$.

(c) The fold changes in event frequency following depolarization.

(d-f) Data obtained from GFP- astrocytes and GFP- neurons. $p=0.24$, $n=7$.

(g-i) Data obtained from GFP+ astrocyte and GFP- neuron pairs. $p= 0.02$, $n=8$.

(j-l) Data obtained from GFP- astrocytes and GFP+ neurons. $p= 0.1176$, $n=10$.



similar to the global null male mice. In the third combination, depolarization of a MeCP2-positive astrocyte increased the frequency of synaptic currents in a neighboring MeCP2-negative neuron by 1.66 ± 0.25 fold (Pre: 189 ± 02 events/min, Post: 268 ± 96 events/min, $p= 0.02$, $n=8$) (figure 20i- h). However, when a MeCP2-negative astrocyte was paired with a MeCP2-positive neuron, depolarization resulted in no significant increase in the frequency of synaptic currents (Pre: 176 ± 81 events/min, Post: 188 ± 83 events/min, $p= 0.1176$, $n=10$) (figure 20k, l). These experiments indicate that the astrocyte, not the neuron, must express MeCP2 in order to have a significant effect on astrocyte-mediated signaling within the local circuit.

Purinergic rescue of MeCP2-deficient astrocyte-mediated signaling

Recent studies from both RTT patients and RTT mouse models have found sufficient evidence implicating oxidative stress, due to reactive oxygen species, in the dysfunctions observed in RTT (Filosa et al., 2015). Data has shown that impaired complex II from the mitochondrial respiratory chain induces H_2O_2 overproduction and decreased mitochondrial ATP synthesis in RTT mouse brains (DeFilippis et al., 2015). To investigate whether restoring ATP levels in RTT astrocytes rescues the lack of astrocyte-mediated modulation of neuronal signaling, MeCP2-null astrocytes were dialyzed with 5mM ATP and the effect of astrocyte activation on the frequency of synaptic currents was quantified. Surprisingly, TFLLR application, after astrocytes were dialyzed with ATP, significantly increased the

frequency of synaptic currents in proximal neurons by 1.4 fold (Pre TFLLR: 268 ± 151 events/min, Post TFLLR: 353 ± 162 events/min, $p= 0.0078$, $n=8$) (figure 21a, b). To determine whether ATP was being consumed by the astrocyte for metabolic purposes, ATP dialysis, and subsequent astrocyte activation, was repeated in the presence of the purinergic receptor antagonist PPADS ($100\mu\text{M}$). By blocking ATP receptors, TFLLR application with ATP dialysis produced no increase in the frequency of synaptic events (Pre TFLLR: 129 ± 77 events/min, Post TFLLR: 136 ± 94 events/min, $p= 0.595$, $n=7$) (figure 21c, d). These data suggest that the “rescue” achieved by dialyzing RTT astrocytes with ATP was due to the astrocyte releasing the ATP rather than using it in intracellular processes.

Figure 21. Dialyzing MeCP2-null astrocytes with ATP results in astrocyte-mediated modulation of neuronal signaling through the release of ATP onto neuronal purinergic receptors.

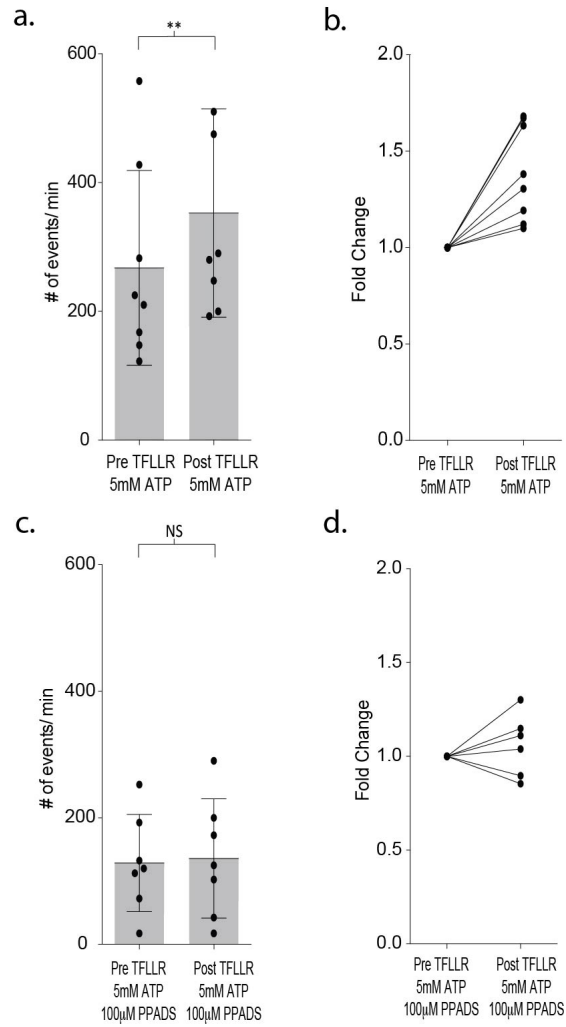
(a) The frequency of synaptic currents was quantified before and after 500 μ M TFLLR was applied to astrocytes dialyzed with 5mM ATP, grey box indicates mean \pm SD (Pre TFLLR: 268 \pm 151 events/min, Post TFLLR: 353 \pm 162 events/min, p= 0.0078, n=8)

(b) The corresponding fold-change for the individual recordings in (a).

(c) 500 μ M TFLLR was applied to astrocytes dialyzed with 5mM ATP in the presence of 100 μ M PPADS, grey box indicates mean \pm SD (Pre TFLLR: 129 \pm 77 events/min, Post TFLLR: 136 \pm 94 events/min, p= 0.595, n=7)

(d) The corresponding fold-change for the individual recordings in (c).

Symmetrical chloride internal was used, neurons voltage clamped at -80mV



Lack of astrocyte-mediated signaling is not due to SR101 treatment

SR101 treatment has been an essential tool in identifying astrocytes *in vivo*. However, it has been reported that use of SR101 can have severe excitatory effects on neurons such as lowering the threshold for action potential generation (Kang et al., 2010), seizure-like activity (Rasmussen et al., 2016), and induction of LTP (Kang et al., 2010). To ensure that the lack of astrocyte-mediated effects in MeCP2 null animals is not due a toxic SR101 interaction with MeCP2-null astrocytes, the concentration of SR101 used in my recordings (100nM) was well below the levels found to induce excitation (1 μ M to 100 μ M). Nevertheless, I repeated astrocyte-neuron recordings without SR101 to confirm that the lack of astrocyte-mediated effects was not due to the staining. Layer 2/3 astrocytes were first identified by locating vasculature in the slice, being that astrocyte end-feet wrap blood vessels to maintain the integrity of the blood brain barrier, cells with small somas (~10 μ m) were targeted as potential astrocytes. Second, upon achieving patch-clamp configuration, astrocytes were further identified by their lack of sodium current. Third, an Alexa Fluor dye was included in the patch pipette to fill the cell, further identifying hallmark multipolar anaxonic astrocyte morphology and spread of dye within astrocyte network (figure 22a). Once confirmed as an astrocyte, the cell was depolarized as before (figure 2 and figure 16a- f) and the effect on the frequency of synaptic currents was measured. Repeating astrocyte depolarization without SR101 still found no effect on the frequency of synaptic currents (Pre depolarization: 147 \pm 54 events/min, Post depolarization: 161 \pm 63 events/min, p= 0.109, n=8) (figure 22b, c), indicating SR101 was not having an adverse effect on MeCP2 null astrocytes.

Figure 22. SR101 treatment does not affect the lack of astrocyte-mediated signaling in MeCP2 null barrel cortex

(a) Left: DIC image of paired astrocyte-neuron recording configuration. Middle: Alexa fluor fill of astrocyte and spread of dye within astrocyte network. Right: Neuron fill to demonstrate noticeable difference in morphology from astrocyte. Exposure time of photo was increased to delineate astrocytic processes. Scale bar is 20 μ m.

(b) The frequency of synaptic currents was quantified before and after astrocyte depolarization, grey box indicates mean \pm SD (Pre depolarization: 147 \pm 54 events/min, Post depolarization: 161 \pm 63 events/min, p= 0.109, n=8)

(c) The corresponding fold-change for the individual recordings in (b).

Chapter 5

The role of calcium in astrocyte-neuron signaling

The finding that astrocytes directly respond to stimuli with rises in intracellular calcium changed the qualification of the astrocyte from a support cell into a cell type capable of independently processing information. Specifically, it was early experiments where the application of glutamate to astrocytes in culture, in slices, in the whole retina, and *in vivo* was found to induce intracellular calcium signals that could spread between astrocytes (Cornell-Bell et al., 1990; Dani et al., 1992; Porter et al., 1996; Newman & Zahs, 1997; Hirase et al., 2004; Nimmerjahn et al., 2004). The relevance of astrocytic calcium signals to neuronal processing was established when they were found to precede neuronal calcium signals (Parpura et al., 1994; Nedergaard, 1994). This exciting work created a new perspective on astrocytic function centered on “gliotransmission”, where stimulation of astrocytes lead to the release of “gliotransmitters” that could act directly on neurons and modulate their activity (Hamilton & Attwell, 2010; Halassa and Haydon, 2010; Araque et al., 2014). In order to study the role of astrocytic calcium in the modulation of neuronal signaling in both wild type and RTT mice, I utilized calcium imaging and calcium uncaging. Calcium imaging allowed me to survey differences in the calcium responsiveness of MeCP2-deficient and MeCP2-expressing astrocytes and neurons to different agonists, whereas calcium uncaging was used to determine if calcium was sufficient to trigger astrocyte-mediated modulation.

Intracellular calcium is required for astrocyte-mediated effects

To determine whether intracellular calcium signaling was required for the astrocyte-mediated signaling with neurons, I dialyzed WT astrocytes with a calcium buffer to clamp intracellular calcium to low levels. The astrocytes were identified on the basis of SR101 labeling and dialyzed with the calcium buffer along with fluorescent Alexa Fluor 488 (figure 23a). Green fluorescence was monitored to insure complete dialysis prior to TFLLR application. The intracellular calcium was clamped to low resting levels in astrocytes using either calcium free-10mM BAPTA (figure 23b black symbols) or a calcium-BAPTA buffer corresponding to 100 nM free calcium (figure 23b red symbols). After 15 minutes of dialysis via the astrocyte patch pipette, TFLLR (500 μ M) was locally applied while the frequency of events was determined for a proximal neuron. Dialysis with either BAPTA buffer reduced the basal frequency of neuronal events from the collective pre-stimulus levels by 0.72 ± 0.08 fold, along with no further increase in frequency following TFLLR application ($p=0.02$, $n=10$) (figure 23b, c). The finding that the frequency of synaptic events was reduced upon activation of BAPTA-loaded astrocytes may be explained by the additional diffusion of BAPTA into the astrocytic network over time, which is supported by the spread of Alexa Fluor dye into neighboring astrocytes (figure 23a, right). In addition, TFLLR may also have inhibitory off-target effects that are normally masked by the potent astrocyte-mediated increase in frequency. Nevertheless, these data show that the increase in neuronal signaling found after astrocyte activation requires intracellular calcium levels in astrocytes to support the astrocyte/neuron signaling.

Figure 23- Clamping calcium to low intracellular levels prevents the TFLLR astrocyte mediated increase in neuronal event frequency.

(a) Images showing the DIC (left), SR101 label (middle) and the Alexa 488 fill (right) of the astrocyte. Note spread of Alexa 488 within astrocyte network. Photo taken before puffer pipette was brought into frame.

(b) The mean event frequency from each neuron recording pre and post-application of 500 μ M TFLLR. $p=0.02$, $n=10$. The 10mm BAPTA recordings are shown in black and the calcium BAPTA recordings are shown in red.

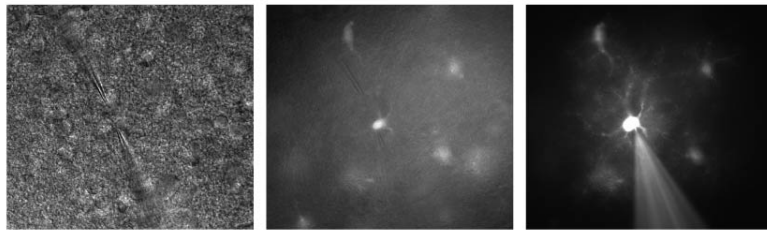
(c) The fold change for the recordings in b.

a.

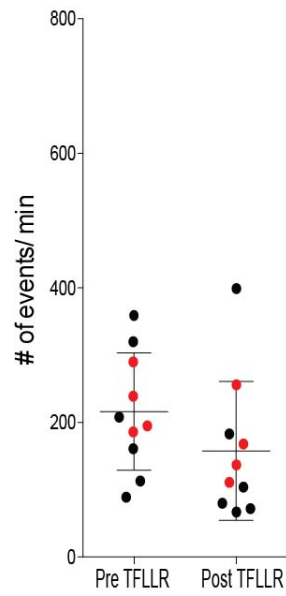
DIC

SR101

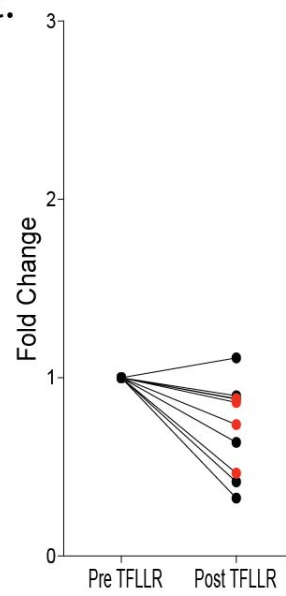
Alexa488



b.



c.



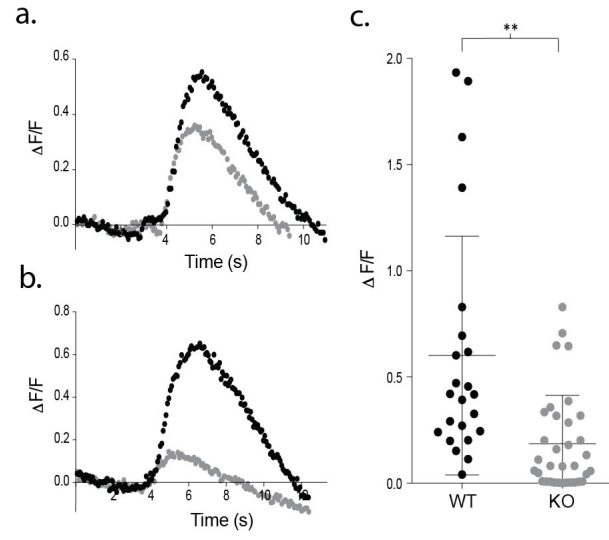
Intracellular calcium signaling is deficient in MeCP2 null astrocytes

Calcium indicators were used to test for defects in intracellular calcium signaling in MeCP2-deficient astrocytes. For this purpose, WT cortical slices were incubated with Fluo4FF-AM (10 μM ; $K_D=9.7 \mu\text{M}$) for 35 minutes, which preferentially loaded SR101 positive astrocytes. The calcium signal in resting astrocytes was weak but reliable somatic increases in calcium were seen in response to TFLLR application (figure 24a). The somatic signals were quantitated on the basis of background corrected $\Delta F/F_0$ signals. WT astrocytes produced rises in somatic calcium signals within one second of TFLLR application that required several seconds for complete relaxation to resting values (figure 24a, b). The overall mean for individual experiments corresponded to a $\Delta F/F_0$ of 0.60 ± 0.56 (figure 24c; $n=23$). Using the global MeCP2 null mice, 18 out of 29 tests of MeCP2 deficient astrocytes produced detectable calcium signals in response to TFLLR application (figure 24). In those 18 cases where responses were detected, the calcium signals followed a time course similar to WT (figure 24a, b) but were significantly lower in intensity (mean $\Delta F/F_0= 0.19 \pm 0.12$, $n=18$) ($p= 0.002$) (figure 24c).

Figure 24- Measurement of intracellular calcium reveals blunted responses to TFLLR application in MeCP null astrocytes.

(a,b). Two sample data sets showing $\Delta F/F_0$ measurements from WT astrocytes (black) and MeCP null astrocytes (gray) during a round of TFLLR application. The top example reflects one of the strongest KO responders and the bottom example is representative of the overall mean. The time courses for WT and KO are similar and the dip below baseline following recovery reflects the time-dependent bleaching of the calcium indicator.

(c) The scatterplot of $\Delta F/F_0$ for individual recordings comparing WT and KO. Mean \pm SD for the overall data are indicated



As a positive control, calcium responsiveness of MeCP2 null cortical neurons was then tested by application of 500 μ M glutamate, which acts on both astrocytes and neurons. Glutamate (500 μ M) application produced robust calcium responses in both WT astrocytes ($\Delta F/F_0=0.63 \pm 0.56$, n=7) and neurons ($\Delta F/F_0= 1.71 \pm 1.16$, n=11) (figure 25). When MeCP2 deficient slices were tested, glutamate application produced similar calcium responses in MeCP2 null neurons ($\Delta F/F_0=1.52 \pm 1.30$, p=0.70, n=7), but astrocytic signals were significantly reduced compared to WT astrocytes (3/9 had no response, of the 6 responders $\Delta F/F_0= 0.20 \pm 0.098$, p=0.035). These data indicate that calcium signaling is normal in MeCP2 null neurons, but is specifically reduced in MeCP2 null astrocytes.

Figure 25: Measurement of calcium responses to glutamate application reveals that MeCP2-null neurons do not have defective calcium responses compared to WT neurons whereas MeCP2-null astrocytes had reduced calcium responses to glutamate application when compared to WT astrocytes.

(a) Representative calcium signals from 500 μ M glutamate application (at 4sec) in a WT neuron (black) and a MeCP2 null neuron (grey).

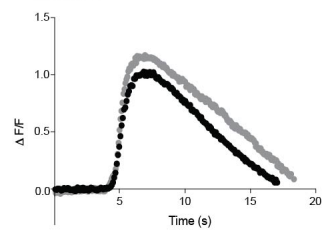
(b) Representative calcium signals from 500 μ M glutamate application (at 4sec) in a WT astrocyte (black) and a MeCP2 null astrocyte (grey).

(c) Cumulative data for $\Delta F/F_0$ calcium signals for WT neurons (n=11) and MeCP2 null neurons (p=0.70, n=7).

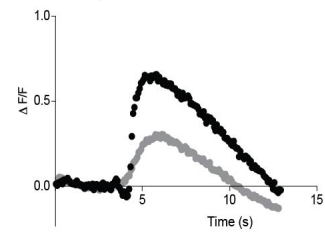
(d) Cumulative data for $\Delta F/F_0$ calcium signals for WT astrocytes (p=0.035, n=6) and MeCP2 null astrocytes (n=9).

All cells bulk loaded with 10 μ M Fluo4-AM.

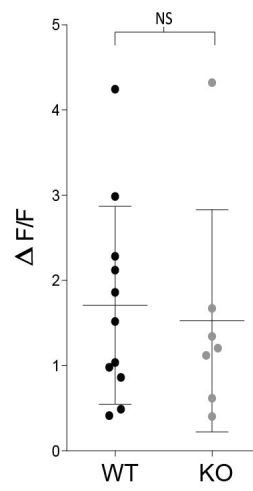
a. Neuron



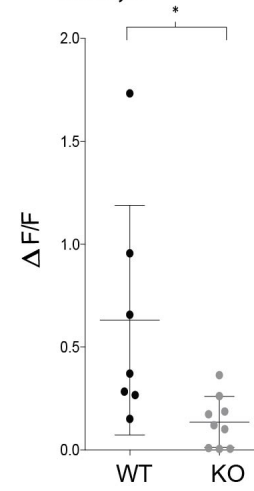
b. Astrocyte



c. Neuron



d. Astrocyte



Restoring intracellular calcium is not sufficient to rescue MeCP2 null astrocytes

Finally, I tested whether restoring intracellular calcium levels in MeCP2 deficient astrocytes was able to trigger astrocyte-mediated neuronal signaling. To do this I loaded an astrocyte with DMNP-EDTA caged calcium (4mM DMNP-EDTA, 3.6mM CaCl₂) for 10 minutes via the patch pipette. Calcium was then uncaged in the astrocyte via a 1 sec LED light flash (figure 26a) while the frequency of synaptic currents in the neighboring neuron was recorded. To ensure that this uncaging protocol was effectively increasing intracellular calcium, I also bulk loaded WT slices with the calcium indicator Fluo4FF-AM. Photolysis in astrocytes effectively increased the somatic calcium levels for both WT ($\Delta F/F_0 = 0.18 \pm 0.06$, n=6) and KO ($\Delta F/F_0 = 0.26 \pm 0.05$, n=4) (figure 27). In WT slices, uncaging of calcium loaded DMP-EGTA resulted in an average 1.39 ± 0.08 fold increase in the frequency of synaptic currents in the neighboring neuron (Pre: 250 ± 94 events/min, post: 326 ± 75 events/min, p= 0.0003, n=16) (figure 26b). The response was similar to that observed in depolarization-based and agonist-based experiments in terms of onset and duration (figure 26c). In control experiments, photolysis of WT astrocytes dialyzed with an empty cage did not alter the frequency of synaptic currents (pre: 109 ± 66 events/min, post: 115 ± 75 events/min, n=4) (figure 27). When uncaging was repeated using MeCP2 null slices (figure 26d), there was no significant change in the frequency of synaptic currents (Pre: 227 ± 112 events/min, Post: 237 ± 121 events/min, p=0.23, n=16) (figure 26e, f).

Figure 26. Uncaging intracellular calcium does not rescue astrocyte-neuron signaling.

(a) Sample recordings from a neighboring WT cortical neuron before (upper) and after (lower) flash uncaging of intracellular calcium in the WT astrocyte.

(b) The scatterplot of pre and post-flash responses showing the mean (shaded) and SD. $p=0.0003$, $n=16$

(c) The associated fold change for each of the measurements shown in b.

(d-f) Measurements made from MeCP2 null neurons when MeCP2 null astrocytes were loaded with caged calcium showing, in all but one recording, no significant increase in neuronal event frequency upon uncaging of calcium. $p=0.23$, $n=16$.

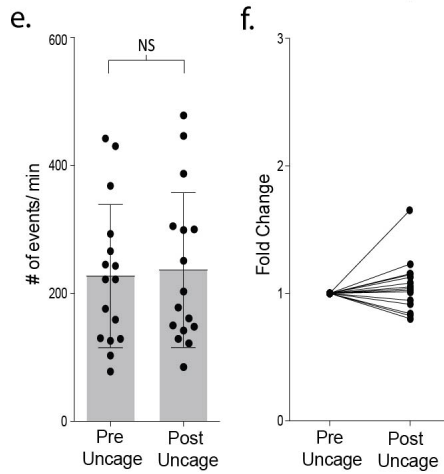
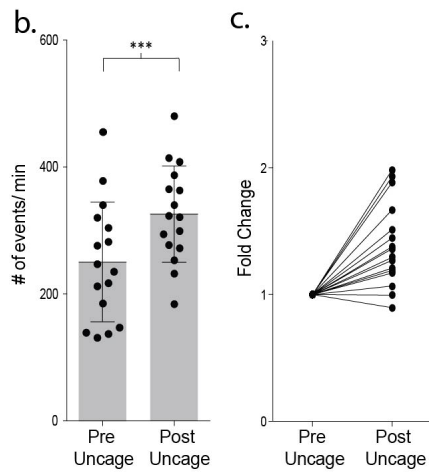
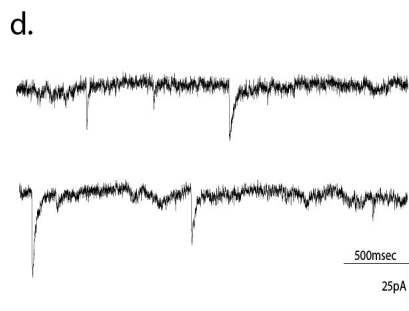
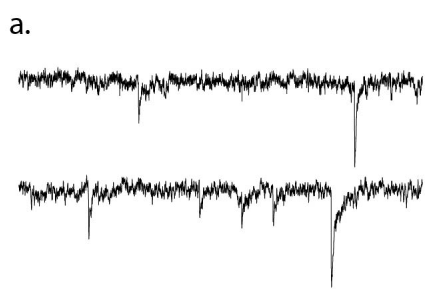


Figure 27: Fluo4FF-AM calcium imaging of astrocytic somatic calcium signals ($\Delta F/F_0$) from photolysis of DMNP-EDTA caged calcium in WT and MeCP2 null slices. Slices were incubated in Fluo4FF-AM and DMNTP-EDTA caged calcium was subsequently loaded in the astrocyte via patch pipette.

(a) Representative calcium signal from photolysis at 2 sec in WT astrocyte (black).

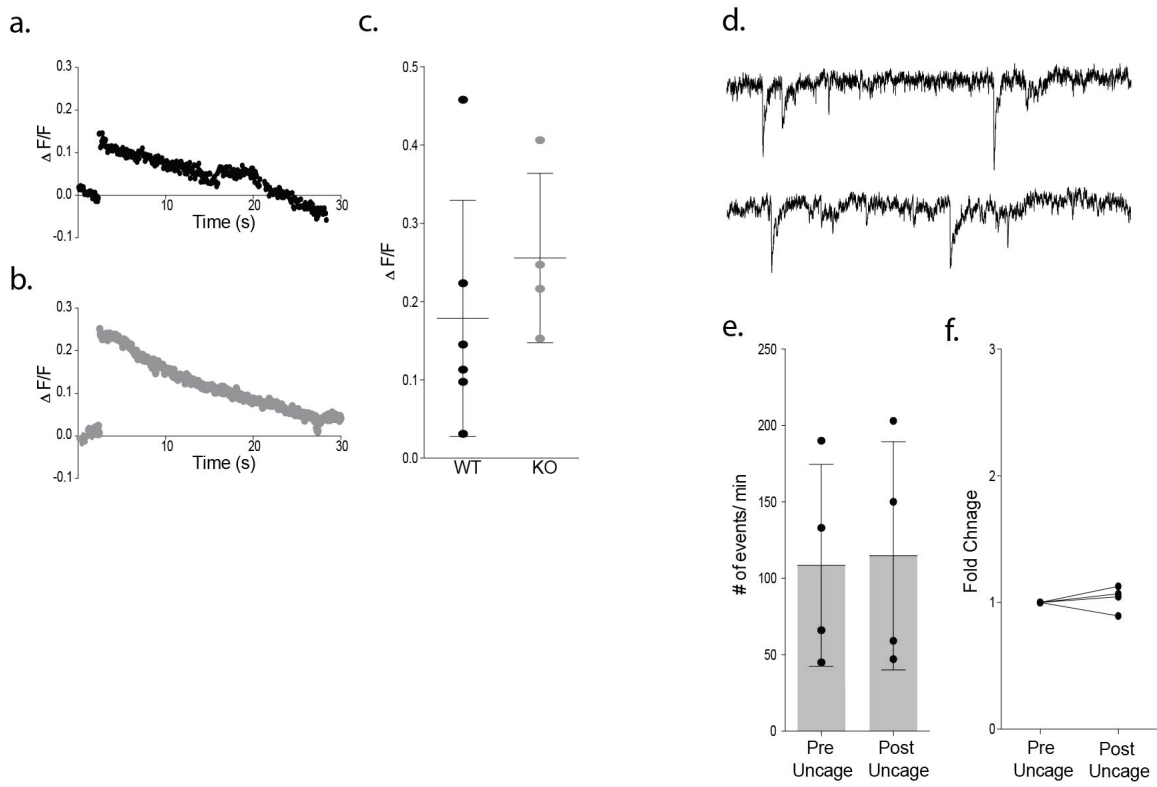
(b) Representative calcium signal from photolysis at 2 sec in MeCP2-null astrocyte (grey).

(c) Cumulative data from WT and MeCP2 null astrocytes showing photolysis protocol effectively increased the somatic calcium levels for both WT ($\Delta F/F_0 = 0.18 \pm 0.06$, n=6) and KO ($\Delta F/F_0 = 0.26 \pm 0.05$, n=4)

(d) Representative traces before and after photolysis of an astrocyte loaded with an empty DMNP-EDTA cage.

(e) Cumulative data showing frequency of events before and after uncaging with empty cage.

(f) Fold change for data shown in e.



Chapter 6

Discussion

Astrocytic modulation of neuronal signaling in wild type mouse barrel cortex

There is precedent from both electrophysiological and calcium measurements for the ability of astrocyte stimulation to affect neuronal function in the brains of healthy mice (Nedergaard et al., 1994; Kang et al., 1998; Fellin et al., 2004; Perea & Araque, 2005; Jourdain et al., 2007; Martín et al., 2015 Schipke et al., 2008; Benedetti et al., 2011; Min & Nevian, 2012). This thesis contributes to what is known about astrocyte-neuron signaling in barrel cortex. Whereas previous work has focused on either glutamate-mediated plasticity or GABA-mediated inhibition in the mature mouse brain, this study offers an in depth look at how astrocytes modulate both glutamatergic and GABAergic neuronal signaling in the young mouse brain. Using electrophysiological recordings and calcium imaging, my data supports that astrocyte-mediated effects are strongest within the spatial domain (~20 μ m area around the soma) of an astrocyte and that astrocyte-mediated effects require intracellular calcium signaling. However, my data challenges the role of GABA as the sole gliotransmitter modulating synaptic transmission in layer 2/3 of barrel cortex. In the following section I will address the application of my results to astrocyte-mediated signaling within the spatial domain of an astrocyte, identification of

gliotransmitters in barrel cortex, and the role of calcium in astrocyte-mediated modulation of neuronal signaling in barrel cortex at p10-p12.

Astrocyte-neuron signaling was studied in this dissertation by combining multiple forms of astrocyte stimulation with neuronal electrophysiological recordings. By applying different modes of astrocyte-specific stimulation that all resulted in the up-regulation of neuronal transmission, each stimulus modality uncovered different signaling cascades within the astrocyte that mediate gliotransmission in barrel cortex. Direct depolarization of the astrocyte using a patch pipette works via either voltage-gated channels or voltage-sensitive transporters, puffer application of an astrocyte-specific agonist (TFLLR) of the protease-activated receptor 1 (Par1) works through G_q -coupled signaling (PLC/IP₃/ER-store), and calcium-uncaging acts directly on release machinery by increasing intracellular calcium. All three forms of stimulation triggered astrocyte-mediated effects and led to an increase in frequency of synaptic currents, supporting a role for astrocytes in the modulation of neuronal signaling in barrel cortex at p10-p12.

In order to study the signaling within the spatial domain of barrel cortex astrocytes, triple-electrode recordings were used. The spatial domain of each astrocyte was identified by the limits of the astrocyte's processes, delineated using SR101 fluorescence. Neurons that were proximal (within the SR101-positive processes) and distal (varying distances outside the SR101-positive processes) to an astrocyte were voltage clamped and astrocyte depolarization ensued. Quantification of astrocyte-mediated effects found that modulation was strongest in the proximal neuron (<20 μ m) and decreased as a function of distance (effects were minimal at

40 μ m from soma). This finding is important for our understanding of communication within the astrocytic network, because it suggests that though astrocytes form an interconnected network, the study of intercellular astrocyte-neuron signaling must be done with proximity taken into consideration. A false negative could easily be reported simply because the neuron lies outside of the spatial domain of the astrocyte.

Having established the localization of astrocyte-mediated effects, I sought to identify direct astrocyte-to-neuron chemical transmission within the spatial domain ($\sim 20\mu$ m). As the frequency of synaptic events increases as a result of astrocyte depolarization, the timing of synaptic events in relation to astrocyte depolarization could potentially be used to study the release process following astrocyte activation. The data show that within 200msec, astrocyte depolarization increased the frequency of synaptic currents, however the frequency was not affected until 40msec after depolarization and was maximal at 60msec. This latency in onset indicates that astrocyte-mediated modulation of neuronal signaling is not mediated through monosynaptic contact (Regehr and Sabatini, 1997). To account for the latency, I tested whether the recruitment of multiple presynaptic neurons was involved in astrocyte-mediated effects. Repeating both depolarization-based and agonist-based astrocyte stimulation in the presence of TTX to block neuronal action potentials prevented the astrocyte-mediated increase in frequency of synaptic events, indicating that astrocyte-mediated effects requires activation of neurons. To determine directly whether more than one neuron type was recruited, the neuronal transmitters underlying the astrocyte-evoked synaptic currents were identified

using pharmacology. Indeed, the recruitment of more than one kind of neuron was validated by the evidence for modulation of both glutamatergic and GABAergic signaling. Glutamate mediated currents increased 1.7 fold after astrocyte stimulation and GABA mediated currents increased 1.6 fold. Being that neurons in barrel cortex have not been reported to co-release GABA and glutamate (Hnasko and Edwards, 2012) and considering the onset latency of astrocyte-mediated effects, the TTX sensitivity, and the increase of both GABAergic and glutamatergic signaling, these data suggest that astrocyte activation results in the recruitment of all neurons within the spatial domain, regardless of their identity.

A central question involving the astrocyte-mediated effects on neuronal physiology is the nature of the factor(s) released by the astrocyte that are causal to the initiation of neuronal synaptic signaling. Identifying that GABA receptors and glutamate receptors mediate the majority of the neuronal signaling affected by astrocyte activation was problematic for the identification of the gliotransmitter, given that both GABA (Benedetti et al., 2011) and glutamate (Min & Nevian, 2012) themselves have been reported as chemical signals released by astrocytes in barrel cortex. In order to determine the glutamatergic and GABAergic contributions in astrocytic chemical transmission, I had to find a way to separately monitor both GABA receptor and glutamate receptor mediated currents at the same time. For this purpose, I used a low-chloride internal solution that allowed me to take advantage of the subsequent bi-directionality of mainly GABA receptor (outward) and glutamate receptor (inward) mediated currents to test for the specific roles of either of these common gliotransmitters. GABA was first ruled out as the gliotransmitter,

as well as the upstream requirement for activation of GABAergic neurons by the astrocyte, on the basis of continued agonist-induced increases in inward current frequency in the presence of gabazine. By contrast, no statistically significant increase in either inward or outward current frequency was observed in the presence of glutamate receptor blockers, consistent with glutamate representing the gliotransmitter. However, given that there were a substantial numbers of recordings that still showed prominent increases in outward current in the presence of glutamate receptor antagonists, the results remain inconclusive. This persistence of astrocyte-mediated effects suggests that an additional gliotransmitter may be involved. For example, ATP is also known to be released by astrocytes (Serrano et al., 2006; Bal-Price et al., 2002; Newman, 2003; Chen et al., 2013; Pascual et al., 2005; Gourine et al., 2010; Bowser and Khakh, 2004), but has not yet been implicated in astrocyte-mediated signaling in barrel cortex. To address the contribution of purinergic signaling, astrocyte activation was repeated in the presence of a P2-receptor antagonist. Blocking extracellular ATP signaling did not prevent the increase in outward current frequency after astrocyte stimulation, indicating that the release of ATP from the astrocyte, as well as the potential upstream requirement of ATP release from neurons, is not required for astrocyte-mediated signaling in barrel cortex.

Intracellular calcium has been implicated in astrocyte-mediated signaling in adult barrel cortex (Benedetti et al., 2011; Min and Nevian, 2012; Perez-Alvarez et al., 2014; Takata et al., 2011). To determine if intracellular calcium was also involved in astrocyte-mediated modulation of neuronal signaling in barrel cortex at

p10-p12, I adopted three approaches. First, calcium imaging verified that activation of the G_q-coupled par1 receptor with TFLLR resulted in increases in intracellular calcium levels, second, buffering calcium to low levels in astrocytes with BAPTA blocked astrocyte-mediated effects, and third, uncaging calcium in astrocytes was sufficient to trigger astrocyte-mediated modulation of neuronal signaling. Whereas the calcium imaging data does not directly indicate causality between a rise in astrocyte calcium levels and the subsequent effects on neuronal signaling, both the BAPTA and calcium uncaging experiments do support causality. Dialyzing astrocytes with the calcium buffer BAPTA also reduced the basal frequency of neuronal synaptic currents. This BAPTA-mediated reduction in the basal frequency of synaptic currents suggests that astrocytes may be contributing to a tonic signaling tone in barrel cortex, which has been reported in other brain regions (cerebellum: Lee et al., 2011; visual cortex: Poskanzer and Yuste, 2016; hippocampus: Pascual et al., 2005). Furthermore, this reduction in basal frequency may be the result of BAPTA diffusion into the astrocytic network via gap junctions, which has been shown to affect astrocytes within 200 μ m (Benedetti et al., 2011). By effectively shutting down neighboring astrocytes, BAPTA dialysis would reduce astrocyte-mediated excitation of neighboring neurons at a larger scale. Taken together, these experiments confirm the importance of astrocyte calcium signaling in barrel cortex.

The data presented in my thesis largely support previous publications involving astrocyte-mediated effects in adult barrel cortex. First, my triple-electrode recordings support the modeling and structural studies that, based on the morphology of astrocytic processes, suggest astrocyte-neuron signaling is strongest

within the spatial domain of the activated astrocyte (Mitterauer, 2010; Oberheim et al., 2006, Oberheim et al., 2008, Schipke et al., 2008). This was directly tested and confirmed in my study; astrocyte-mediated effects at p10-p12 were strongest within 20 μ m of the astrocyte soma and were reduced at distances over 40 μ m. Second, my experiments measuring and manipulating astrocytic intracellular calcium (calcium imaging, BAPTA-mediated buffering, and calcium uncaging) support the importance of calcium signaling in astrocyte-mediated processes in barrel cortex. My data, specifically the BAPTA-mediated buffering of calcium and calcium uncaging, supports a causal role of calcium in astrocyte-mediated effects, which has been reported to mediate barrel cortex plasticity induced by sensory stimuli (Lind et al., 2013; Benedetti et al., 2011; Min and Nevian, 2012; Perez-Alvarez et al., 2014; Takata et al., 2011; Schipke et al., 2008). Third, whereas previous publications have identified effects on either glutamate-mediated plasticity (Min and Nevian, 2012; Poskanzer and Yuste, 2016) or GABA-mediated inhibition (Benedetti et al., 2011) in barrel cortex, my data provides evidence for astrocytic modulation of both glutamate and GABA in barrel cortex. This result is particularly interesting given reports from barrel cortex and striatum that astrocytes can discriminate and selectively respond to the activity of specific neurons (Schipke et al., 2008; Martín et al., 2015, respectively), because it suggests that even though afferent input is preferentially driving certain astrocytes, downstream signaling from the astrocyte is indiscriminant, increasing all neuronal activity within the spatial domain of that astrocyte. Fourth, my data challenges the notion that GABA is released from astrocytes in barrel cortex (Benedetti et al., 2011) and supports the release of a

chemical activating glutamate receptors (glutamate or d-serine), which has been well documented in barrel cortex (Min and Nevian, 2012; Takata et al., 2011).

Taken together, the experiments in this thesis allow for the construction of the following model: Astrocyte activation results in elevated intracellular calcium, facilitating either astrocytic vesicle fusion or release through a calcium-activated anion channel, where an excitatory chemical signal is released and subsequently drives release from neuronal terminals within the spatial domain of the activated astrocyte. The simplest astrocyte-neuronal network supported by this model consists of a stimulated astrocyte, the neuron under recording, and release from both a GABAergic and a glutamatergic neuron. Based on pharmacological manipulations and the simultaneous monitoring of cation-mediated and anion-mediated currents, the excitatory drive on the neuronal network following astrocyte activation involves either direct release of glutamate from the astrocyte or release of an excitatory chemical signal from the astrocyte that drives glutamate-release from a glutamatergic neuron that subsequently stimulates release from GABAergic terminals and additional glutamatergic terminals within the spatial domain of the activated astrocyte. The contribution of GABA and ATP, emanating from either the astrocyte or upstream neurons, was not required for astrocyte-mediated effects, being that astrocyte-mediated effects persisted in the presence of the respective receptor antagonists.

In conclusion, my work on astrocyte-mediated processes in young wild type barrel cortex indicates that upon activation, astrocytes are capable of modulating

neuronal signaling. Being that this signaling is present in the healthy mouse brain, the relevance of astrocyte-mediated effects in disease states is of interest.

Astrocytic modulation of neuronal signaling in a mouse model of Rett syndrome

Recent studies have drawn into question the exclusive role of neurons in the progression of Rett syndrome (RTT), a disease resulting from the loss of MeCP2 expression in 50% of the cells comprising the brain. For example, the progression of overt RTT-like behaviors in mice was ameliorated following postnatal restoration of MeCP2 in astrocytes, consistent with the reversibility of the disease (Guy et al 2007; Liou et al., 2011). Additionally, RTT astrocytes have been shown to have negative effects on the development of neurons in co-culture experiments (Ballas et al., 2009; Williams et al., 2014), reduced sensitivity to the direct detection of carbon dioxide (Turovsky et al 2015; Garg et al., 2015), and aberrant microtubule (MT) dynamics and vesicular transport (Delepine et al., 2016). Given the defects associated with loss of astrocytic MeCP2, I sought to investigate how loss of MeCP2 affects astrocyte-mediated modulation of neuronal signaling in barrel cortex.

My astrocyte-neuron recordings using barrel cortex slices from global MeCP2-null male mice revealed greatly reduced astrocyte-mediated modulation of the frequency of synaptic currents. Specifically, neither astrocyte depolarization nor agonist application had a significant effect on the frequency of synaptic currents. This lack of astrocyte-mediated effects occurred even though the expression of par1 was no different from wild type levels, and that basal neuronal GABAergic and

glutamatergic signaling was similar to wild type. Given the non-cell autonomous effects of RTT astrocytes on neurons, it was important to determine if this lack of astrocyte-mediated signaling was due to loss of MeCP2 expression in the astrocyte, the neuron, or both cell types. To address this, I utilized heterozygous mutant female mice that are mosaic for loss of MeCP2 due to X-chromosome inactivation. Further, these mice contain a knockin of GFP into the endogenous *Mecp2* gene, such that in the heterozygous condition, only the WT cells are fluorescent. Thus, MeCP2-GFP was expressed in ~50% of all neurons and astrocytes, whereas the remaining 50% of the cells expressed a truncated, nonfunctional MeCP2 protein (Lyst et al., 2013). These MeCP2-GFP heterozygous mice provided the opportunity to record from all pairwise combinations of WT (GFP-positive) and RTT (GFP-negative) astrocytes and neurons, which reflects the same condition as in human females with RTT. These recordings show that MeCP2 expression in the astrocyte was required for astrocyte-mediated modulation of neuronal signaling, regardless of the neuronal MeCP2 expression. This result indicates that in the female RTT brain, where 50% of astrocytes and neurons are MeCP2-null, normal astrocyte-mediated effects will occur only when a MeCP2-expressing astrocyte is coupled to a neuron. The relevance of this data to RTT biology challenges the neurocentric approach dominating the field, where the very expression of MeCP2 in astrocytes was originally contested. Though neuronal MeCP2 expression is the basis for RTT pathology (Chahrour and Zoghbi, 2007), these data suggest a WT astrocyte can improve the functioning of a RTT neuron in terms of astrocyte-mediated modulation. Conversely, these data also suggest that the lack of astrocytic

contributions resulting from having a RTT astrocyte paired to a RTT neuron would further contribute to the aberrant signaling existing in the RTT brain.

The loss of MeCP2 may be having multiple effects on the astrocyte, however given that astrocyte stimulation did not have a significant effect on the signaling of neurons, I focused on processes related to gliotransmission. Experiments in wild type astrocytes found that intracellular calcium was both required and sufficient for astrocyte-mediated modulation of neuronal signaling; therefore I sought to test for defective calcium handling in RTT astrocytes. I first tested for defective calcium handling by repeated calcium-imaging experiments. I observed that the robust TFLLR-mediated increase in astrocytic somatic calcium seen in WT astrocytes was greatly blunted in RTT astrocytes. This defect in calcium responsive was astrocyte specific because RTT neurons had normal agonist-mediated and depolarization-mediated calcium responses. These data support my findings from mosaic astrocyte-neuron recordings, wherein astrocyte-mediated effects required the astrocytic expression of MeCP2. Furthermore, these data also support *Turovsky et al., 2015* where RTT astrocytes in the brainstem exhibited attenuated calcium responsiveness to endogenous stimuli (high CO₂). However, *Turovsky et al., 2015* also reported that brainstem RTT astrocytes did produce calcium signals in response to exogenous application of ATP, which conflicts with my data from both TFLLR-based and glutamate-based stimuli. A possible explanation for this disparity could be that brainstem astrocytes are specialized for ATP signaling (Gourine et al., 2010) and therefore are more sensitive to purinergic signaling. It would be interesting to test the calcium responsiveness of RTT astrocytes in the brainstem to

glutamate or TFLLR and to test if barrel cortex RTT astrocytes respond to ATP. Regardless, having found defects associated with agonist-mediated increases in astrocytic intracellular calcium, I tested whether directly increasing cytosolic calcium via calcium uncaging would restore astrocyte-mediated signaling in the global null barrel cortex. Interestingly, RTT astrocytes still failed to elicit neuronal signaling in response to calcium uncaging. This result suggests that, in the context of calcium handling, the defect relevant to modulation of neuronal signaling is either downstream of increases in astrocytic intracellular calcium or alternatively that mechanisms in calcium handling are not solely responsible for the lack of astrocyte-mediated effects. For example, the loss of MeCP2 results in global gene expression changes in the brain, affecting intracellular processes that could impact signal transduction, such as MT-instability and vesicle tracking (Delépine et al., 2016), which would still diminish astrocyte-mediated signaling regardless of intracellular calcium. This lack of astrocyte-mediated effects and the attenuation of astrocyte calcium responsiveness in my recordings contribute to the reported astrocyte-mediated neurodevelopmental defects found in co-culture experiments; both implicate aberrant astrocytic secretion and upstream calcium in RTT (Ballas et al., 2009; Yasui et al., 2017; Delépine et al., 2016; Williams et al., 2014; Okabe et al., 2012).

Though the experimental manipulations aimed at identifying the specific defects responsible for the lack of astrocyte mediated effects in RTT mice were not entirely successful, the following model for RTT astrocyte-neuron signaling can be constructed. Agonist application binds receptors on RTT-astrocytes although the

resulting concentration of intracellular calcium is deficient; therefore the downstream calcium-dependent astrocytic vesicle fusion or release through a calcium-activated anion channel was not attainable. Given the lack of RTT-astrocyte-mediated effects upon directly raising intracellular calcium via uncaging, the model must include an additional, extra-calcium defect. Based on recent data suggesting defects in microtubule stability and the associated aberrant vesicle trafficking, astrocyte-to-neuron signaling will be additionally limited by the lack of a ready-releasable pool of vesicles in the astrocyte or from suboptimal insertion of proteins affiliated with gliotransmission (i.e.: calcium-activated anion channels) into the membrane, both due to aberrant vesicle trafficking. However, if transmitter can be released from the RTT astrocyte, astrocyte-mediated modulation of RTT neuronal signaling is possible, as shown when the RTT astrocyte was dialyzed with a high concentration of ATP.

Taken together, these experiments reveal a perturbation in synaptic communication that can account for, in part, the compromised ability of RTT mouse models to perform normal behavioral tasks, as well as the amelioration of RTT-like phenotypes with the restoration of MeCP2 expression in astrocytes. The defects associated with loss of astrocytic MeCP2 potentially have additional implications with regards to the altered excitatory-inhibitory synaptic balance (E/I- balance) reported in RTT (Feldman et al., 2016). Normally, GABA_A switches from excitatory to inhibitory during early postnatal mouse development (Ben-Ari et al., 1989; Obata et al., 1978; Owens et al., 1996; Dammerman et al., 2000). This switch results from the expression of the chloride exporter KCC2, which establishes the asymmetrical

trans-membrane concentration gradient (Blaesse et al., 2009; Ganguly et al., 2001).

In both humans with RTT and RTT mouse models, a delay in the expression of the chloride exporter occurs, thus causing developmental delay in the switch to inhibition (Duarte et al., 2013; Tang et al., 2016; Feldman et al., 2016).

Consequently, the lack of astrocytic contributions to neuronal signaling in RTT indicates that there will be additional defects associated to the E/I- balance that would extend to brain regions that may be at higher risk due to dependence on proper balance between excitation and inhibition.

Summary of Findings

1. WT astrocytes are capable of modulating neuronal signaling in barrel cortex.
2. WT astrocyte stimulation activates both glutamatergic and GABAergic neuronal signaling in barrel cortex.
3. WT astrocytes do not release GABA as gliotransmitter in barrel cortex.
4. Astrocytic modulation of neuronal signaling is deficient in MeCP2 null barrel cortex.
5. Astrocytic expression of MeCP2, not neuronal, is required for astrocyte-mediated modulation of neuronal signaling in MeCP2^{-/eGFP} barrel cortex.
6. Astrocyte-mediated modulation of neuronal signaling is calcium dependent.
7. MeCP2 null astrocytes have deficient calcium responses.
8. MeCP2 null neurons do not show deficits in calcium responsiveness.
9. Defects associated with the lack of astrocyte-mediated modulation of neuronal signaling in MeCP2 null cortex is either downstream of calcium and/or involves mechanisms not directly related to calcium signaling.

References

- Abbott NJ, Patabendige AAK, Dolman DEM, Yusof SR, Begley DJ. 2010. Structure and function of the blood-brain barrier. *Neurobiol Disease* 37, 13–25.
- Akbarian S, Chen RZ, Gribnau J, Rasmussen TP, Fong H, Jaenisch R. 2001. Expression pattern of the Rett syndrome gene MeCP2 in primate prefrontal cortex. *Neurobiol Disease* 8, 784–791
- Bellot-Saez A, Kékesi O, Morley JW, Buskila Y. 2017. Astrocytic modulation of neuronal excitability through K spatial buffering, *Neuroscience & Biobehavioral Reviews*, 77: 87-97
- Amir RE, Van den Veyver IB, Wan M, Tran CQ, Francke U, Zoghbi HY. 1999. Rett syndrome is caused by mutations in X-linked MECP2, encoding methyl-CpG-binding protein 2. *Nature Genetics*. 23 (2): 185–8.
- Araque A, Li N, Doyle RT, Haydon PG. 2000. SNARE protein-dependent glutamate release from astrocytes. *J. Neurosci*. 20, 666–673
- Araque A, Carmignoto G, Haydon PG, Oliet SHR, Robitaille R, Volterra A. 2014. Gliotransmitters Travel in Time and Space. *Neuron*, 81, 728-739
- Araque A, Parpura V, Sanzgiri RP, Haydon PG. 1999. Tripartite synapses: glia, the unacknowledged partner. *Trends Neurosci*. 22, 208–215
- Axelsen LN, Calloe K, Holstein-Rathlou NH, Nielsen MS. 2013. Managing the complexity of communication: regulation of gap junctions by post-translational modification. *Front. Pharmacol*. 4, 130

Ben-Ari Y. 2002. Excitatory actions of gaba during development: the nature of the nurture. *Nature Neuroscience Reviews*. **3**: 728–739.

Ben-Ari Y, Cherubini E, Corradetti R, Gaiarsa JL. 1989. Giant synaptic potentials in immature rat CA3 hippocampal neurones. *Journal of Physiology* London. **416**: 303–325

Bezzi, P. et al. 2004. Astrocytes contain a vesicular compartment that is competent for regulated exocytosis of glutamate. *Nature Neuroscience*. **7**, 613–620.

Ballas N, Liroy DT, Grunseich C, Mandel G. 2009. Non-cell autonomous influence of MeCP2-deficient glia on neuronal dendritic morphology. *Nature Neuroscience*. **12**(3): 311–317.

Bal-Price A, Moneer Z, Brown GC. 2002. Nitric oxide induces rapid, calcium-dependent release of vesicular glutamate and ATP from cultured rat astrocytes. *Glia*. **40**(3): 312–323

Bazargani N, Attwell D. 2016. Astrocyte calcium signaling: the third wave. *Nature Neuroscience*. **19**: 182–189

Benedetti B, Matyash V, Kettenmann H. 2011. Astrocytes control GABAergic inhibition of neurons in the mouse barrel cortex. *Journal of Physiology*, **589** (5) 1159–1172

Blaesse P, Airaksinen MS, Rivera C, Kaila K. 2009. Cation-chloride cotransporters and neuronal function. *Neuron*. **61**(6): 820–838.

Brown AM, Ransom BR (2007) Astrocyte glycogen and brain energy metabolism. *Glia* 55:1263–1271

Bowser DN, Khakh BS. 2004. ATP excites interneurons and astrocytes to increase synaptic inhibition in neuronal networks. *Journal of Neuroscience*. **24**: 8606–8620

Cahoy JD, et al., 2008. A transcriptome database for astrocytes, neurons, and oligodendrocytes: a new resource for understanding brain development and function. *Journal of Neuroscience* 28, 264–278

Chen J, Tan Z, Zeng L, Zhang X, He Y, Gao W, Wu X, Li Y, Bu B, Wang W, Duan S. 2013. Heterosynaptic long-term depression mediated by ATP released from astrocytes. *Glia*. **61**:178–191.

Chen RZ, Akbarian S, Tudor M, and Jaenisch R. 2001. Deficiency of methyl-CpG binding protein-2 in CNS neurons results in a Rett-like phenotype in mice. *Nature Genetics*. 27, 327–331.

Chahrour, M., Zoghbi, H.Y. 2007. The story of Rett syndrome: from clinic to neurobiology. *Neuron* **56**, 422-437.

Chao HT, Chen H, Samaco RC, Xue M, Chahrour M, Yoo J, Neul JL, Gong S, Lu HC, Heintz N, Ekker M, Rubenstein JL, Noebels JL, Rosenmund C, Zoghbi HY. 2010. Dysfunction in GABA signaling mediates autism-like stereotypies and rett syndrome phenotypes. *Nature*. 468:263–269.

Cornell-Bell AH, Finkbeiner SM, Cooper MS, Smith SJ. 1990. Glutamate induces calcium waves in cultured astrocytes: long-range glial signaling. *Science* 247, 470–473

Dammerman RS, Flint AC, Noctor S, Kriegstein AR. 2000. An excitatory GABAergic plexus in developing neocortical layer 1. *Journal of Neurophysiology*. **84**: 428–434

Dani JW, Chernjavsky A, Smith SJ. 1992. Neuronal activity triggers calcium waves in hippocampal astrocyte networks. *Neuron* 8, 429–440

De Filippis B, Valenti D, de Bari L, de Rasmio D, Musto M, Fabbri A. 2015. Mitochondrial free radical overproduction due to respiratory chain impairment in the brain of a mouse model of Rett syndrome: protective effect of CNF1. *Free Radic. Biol. Med.* 83:167–177.

Delépine C, Meziane H, Nectoux J, Opitz M, Smith AB, Ballatore C, Saillour Y, Bennaceur-Griscelli A, Chang Q, Williams EC, Dahan M, Duboin A, Billuart P, Herault Y, Bienvenu T. (2016). Altered microtubule dynamics and vesicular transport in mouse and human MeCP2-deficient astrocytes. *Human Molecular Genetics*. **25**, 146–157.

Duarte ST, Armstrong J, Roche A, Ortez C, Pérez A, O'Callaghan Mdel M, Pereira A, Sanmartí F, Ormazábal A, Artuch R, Pineda M, García-Cazorla A. 2013. Abnormal expression of cerebrospinal fluid cation chloride cotransporters in patients with Rett syndrome. *PLoS One*. 8:e68851.

Feldman D, Banerjee A, and Sur M. (2016). Developmental dynamics of rett syndrome. *Neural Plasticity*. 6154080

Fellin T, Pascual O, Gobbo S, Pozzan T, Haydon PG, Carmignoto G. 2004. Neuronal synchrony mediated by astrocytic glutamate through activation of extrasynaptic NMDA receptors. *Neuron*. **43**: 729–743

Filosa S, Pecorelli A, D'Esposito M, Valacchi G, Hajek J. 2015. Exploring the possible link between MeCP2 and oxidative stress in Rett syndrome. *Free Radic Biol Med.* 88(Pt A):81–90.

Franke H. et al. 2006. Changes in purinergic signaling after cerebral injury involvement of glutamatergic mechanisms? *Int. J. Dev. Neurosci.* 24, 123–132

Fujita, T. et al. 2014. Neuronal transgene expression in dominant-negative SNARE mice. *Journal of Neuroscience.* 34, 16594–16604.

Ganguly K, Schinder AF, Wong ST, Poo M. 2001. GABA itself promotes the developmental switch of neuronal GABAergic responses from excitation to inhibition. *Cell.* **105**: 521–532

Garg SK, Lioy DT, Knopp SJ, Bissonnette JM. 2015. Conditional depletion of methyl-CpG-binding protein 2 in astrocytes depresses the hypercapnic ventilatory response in mice. *Journal of Applied Physiology.* **119**:670–676

Gourine AV, Kasymov V, Marina N, Tang F, Figueiredo MF, Lane S, Teschemacher AG, Spyer KM, Deisseroth K, Kasparov S. 2010. Astrocytes control breathing through pH-dependent release of ATP. *Science.* **329**: 571–575.

Guy J, Hendrich B, Holmes M, Martin JE, Bird A. 2001. A mouse *Mecp2*-null mutation causes neurological symptoms that mimic Rett syndrome. *Nature Genetics.* **27**(3): 322-6

Guy J, Gan J, Selfridge J, Cobb S, Bird A. 2007. Reversal of neurological defects in a mouse model of Rett syndrome. *Science.* **315**:1143–1147

Halassa MM. et al. 2009. Astrocytic modulation of sleep homeostasis and cognitive consequences of sleep loss. *Neuron* 61, 213–219

Halassa MM, Fellin T, Takano H, Dong JH, Haydon PG. 2007. Synaptic islands defined by the territory of a single astrocyte. *Journal of Neuroscience*. 27, 6473–6477,

Halassa MM, Haydon PG. 2010. Integrated brain circuits: astrocyte networks modulate neuronal activity and behavior. *Annu Rev Physiol* 72, 335–355,

Hamilton NB, Attwell D (2010) Do astrocytes really exocytose neurotransmitters? *Nature Neuroscience Review* 11(4):227–238.

Hirase H, Qian L, Barthó P, Buzsáki G. 2004. Calcium dynamics of cortical astrocytic networks in vivo. *PLoS Biol.* 2, E96

Hirrlinger PG, Scheller A, Braun C, Hirrlinger J.& Kirchhoff F. 2006. Temporal control of gene recombination in astrocytes by transgenic expression of the tamoxifen- inducible DNA recombinase variant CreERT2. *Glia* 54, 11–20

Hnasko TS, Edwards RH. 2012. Neurotransmitter corelease: mechanism and physiological role. *Annu. Rev. Physiol.* 74, 225–243

Hodges MR, Richerson GB. 2008. Interaction between defects in ventilator and thermoregulatory control in mice lacking 5-HT neurons. *Respir Physiol Neurobiol* 164: 350 –357

Hollenberg MD, Saifeddine M, Al-Ani G, Kawabata A. 1997. Proteinase-activated receptors: structural requirements for activity, receptor cross-reactivity, and receptor selectivity of receptor-activating peptides. *Canadian Journal of*

Horner PJ, Power AE, Kempermann G, Kuhn HG, Palmer TD, Winkler J, Thal LJ, Gage FH. 2000. Proliferation and differentiation of progenitor cells throughout the intact adult rat spinal cord. *Journal of Neuroscience*. **20**:2218–2228

Hülsmann S, Hagos L, Heuer H, Schnell C. 2017. Limitations of Sulforhodamine 101 for Brain Imaging. *Frontiers in Cellular Neuroscience*. **11**:44

Jo S, Yarishkin O, Hwang YJ, Chun YE, Park M, Woo DH, Bae JY, Kim T, Lee J, Chun H, Park HJ, Lee DY, Hong J, Kim HY, Oh SJ, Park SJ, Lee H, Yoon BE, Kim Y, Jeong Y, Shim I, Bae YC, Cho J, Kowall NW, Ryu H, Hwang E, Kim D, Lee CJ. 2014. GABA from reactive astrocytes impairs memory in mouse models of Alzheimer's disease. *Nature Medicine*. **20**: 886–896.

Jourdain P, Bergersen LH, Bhaukaurally K, Bezzi P, Santello M, Domercq M, Matute C, Tonello F, Gundersen V, Volterra A. 2007. Glutamate exocytosis from astrocytes controls synaptic strength. *Nature Neuroscience*. **10**, 331–339.

Junge CE, Lee CJ, Hubbard KB, Zhang Z, Olson JJ, Hepler JR, Brat DJ, Traynelis SF. 2004. Protease-activated receptor-1 in human brain: localization and functional expression in astrocytes. *Experimental Neurology*. **188**: 94–103

Kang J, Goldman SA, Nedergaard M. 1998. Astrocyte-mediated potentiation of inhibitory synaptic transmission. *Nature Neuroscience*. **1**, 683–692.

Kifayathullah LA, Arunachalam JP, Bodda C, Agbemenyah HY, Laccone FA, Mannan AU. 2010. MeCP2 Mutant Protein Is Expressed in Astrocytes as well as in Neurons and Localizes in the Nucleus. *Cytogenet Genome Res* **129**: 290–297

Leonard H., Cobb S., Downs J. 2016. Clinical and biological progress over 50 years in Rett syndrome. *Nat. Rev. Neurol.* 13:37–51

Lobsinger CS and Cleveland DW. 2007, Glial cells as intrinsic components of non-cell autonomous neurodegenerative disease. *Nature Neurosci.* 10, 1355-60.

Lee M, McGeer EG, McGeer PL. 2011. Mechanisms of GABA release from human astrocytes. *Glia.* **59**: 1600–1611.

Lee S, Yoon BE, Berglund K, Oh SJ, Park H, Shin HS, Augustine GJ, Lee CJ. 2010. Channel-mediated tonic GABA release from glia. *Science.* **330**: 790–796.

Lewis JD, Meehan R., Henzel WJ, Maurer-Fogy I, Jeppesen P, Klein F, Bird A. 1992. Purification, sequence, and cellular localization of a novel chromosomal protein that binds to methylated DNA. *Cell* 69, 905–914.

Lind B., Brazhe AR, Jessen SB, Tan FC, and Lauritzen M.. (2013). Rapid stimulus-evoked astrocyte Ca²⁺ elevations and hemodynamic responses in mouse somatosensory cortex in vivo. *Proc. Natl. Acad. Sci. U.S.A.* 110, E4678–E4687.

Lioy DT, Garg SK, Monaghan CE, Raber J, Foust KD, Kaspar BK, Hirrlinger PG, Kirchhoff F, Bissonnette JM, Ballas N, Mandel G. 2011. A role for glia in the progression of Rett's syndrome. *Nature.* 475(7357):497–500

Luikenhuis, S., Giacometti, E., Beard, C. F. & Jaenisch, R. 2004. Expression of MeCP2 in postmitotic neurons rescues Rett syndrome in mice. *Proceedings of the National Academy of Sciences USA.* **101** (16): 6033–6038

Lyst MJ, Ekiert R, Ebert DH, Merusi C, Nowak J, Selfridge J, Guy J, Kastan NR, Robinson ND, de Lima Alves F, Rappsilber J, Greenberg ME, Bird A. 2013. Rett

syndrome mutations abolish the interaction of MeCP2 with the NCoR/SMRT co-repressor. *Nature Neuroscience*. **16**: 898–90

Martín R, Bajo-Graneras R, Moratalla R, Perea G, Araque A. 2015. GLIAL CELL SIGNALING. Circuit-specific signaling in astrocyte-neuron networks in basal ganglia pathways. *Science*. 349(6249): 730–4

Meng X, Wang W, Lu H, He LJ, Chen W, Chao ES, Fiorotto ML, Tang B, Herrera JA, Seymour ML, Neul JL, Pereira FA, Tang J, Xue M, Zoghbi HY. 2016. Manipulations of MeCP2 in glutamatergic neurons highlight their contributions to Rett and other neurological disorders. *Elife*. 5:10.7554/eLife.14199.

Min R and Nevian T. 2012. Astrocyte signaling controls spike timing-dependent depression at neocortical synapses. *Nature Neuroscience*. 15, 746–753.

Mitterauer BJ. 2010. Significance of the astrocyte domain organization for qualitative information structuring in the brain. *Adv. Biosci. Biotechnol.* 1, 391–397

Mongin AA & Kimelberg HK. 2005. ATP regulates anion channel-mediated organic osmolyte release from cultured rat astrocytes via multiple Ca²⁺-sensitive mechanisms. *Am. J. Physiol. Cell. Physiol.* 288, C204–C213

Montana V, Ni Y, Hua X, Parpura V. 2004. Vesicular glutamate transporter-dependent glutamate release from astrocytes. *Journal of Neuroscience*. 24, 2633–2642

Nägga K, Bogdanovic N, Marcusson J. 1999. GABA transporters (GAT-1) in Alzheimer's disease. *J. Neural Transm.* 106, 1141–1149

Nan X, Campoy FJ, Bird A. 1997. MeCP2 is a transcriptional repressor with abundant binding sites in genomic chromatin. *Cell* 88, 471–481.

Nedergaard, M. 1994. Direct signaling from astrocytes to neurons in cultures of mammalian brain cells. *Science* **263**, 1768–1771.

Newman, E.A. 2003. Glial cell inhibition of neurons by release of ATP. *Journal of Neuroscience*. **23**: 1659–1666

Newman EA & Zahs KR. 1997. Calcium waves in retinal glial cells. *Science* 275, 844–847

Nimmerjahn A, Kirchhoff F, Kerr JN, Helmchen F. 2004. Sulforhodamine 101 as a specific marker of astroglia in the neocortex in vivo. *Nat. Methods* 1, 31–37.

Nguyen MV, Du F, Felice CA, Shan X, Nigam A, Mandel G, Robinson JK, Ballas N. 2012. MeCP2 is critical for maintaining mature neuronal networks and global brain anatomy during late stages of postnatal brain development and in the mature adult brain. *Journal of Neuroscience*. 32(29): 10021–10034.

Obata K, Oide M, Tanaka H. 1978. Excitatory and inhibitory actions of GABA and glycine on embryonic chick spinal neurons in culture. *Brain Research*. **144**: 179–184

Oberheim NA, Wang X., Goldman S, Nedergaard M, 2006. Astrocytic complexity distinguishes the human brain. *Trends Neurosci*. 29, 547–553,

Oberheim NA, Tian GF, Han X, Peng W, Takano T, Ransom B, Nedergaard M. 2008. Loss of astrocytic domain organization in the epileptic brain. *J. Neurosci*.

28, 3264–3276,

Owens DF, Boyce LH, Davis MB, Kriegstein AR. 1996. Excitatory GABA responses in embryonic and neonatal cortical slices demonstrated by gramicidin perforated-patch recordings and calcium imaging. *Journal of Neuroscience*. **16**: 6414–6423

Parpura V. et al. 1994. Glutamate-mediated astrocyte-neuron signalling. *Nature* 369, 744–747

Pascual O. et al. 2005 Astrocytic purinergic signaling coordinates synaptic networks. *Science* 310, 113–116

Pellerin L, Magistretti PJ. 1994. Glutamate uptake into astrocytes stimulates aerobic glycolysis: a mechanism coupling neuronal activity to glucose utilization. *Proc Natl Acad Sci U S A* 91, 10625–10629.

Perea, G., Araque, A. 2005. Properties of synaptically evoked astrocyte calcium signal reveal synaptic information processing by astrocytes. *The Journal of Neuroscience*. **25**, 2192–2203

Perez-Alvarez A, Navarrete M, Covelo A, Araque A. 2014. Structural and functional plasticity of astrocyte processes and dendritic spine interactions. *Journal of Neuroscience*. 34:12738–12744

Peters A, Palay SL, Webster HD. 1991. The fine structure of the nervous system, Third edn. Oxford University Press, New York

Porter JT & McCarthy KD. 1996. Hippocampal astrocytes in situ respond to glutamate released from synaptic terminals. *Journal of Neuroscience*. 16, 5073–5081

Poskanzer KE, Yuste R. Astrocytes regulate cortical state switching in vivo. *Proc. Natl. Acad. Sci.* 2016;113:E2675–E2684.

Rastegar M, Hotta A, Pasceri P, Makarem M, Cheung AY, Elliott S, Park KJ, Adachi M, Jones FS, Clarke ID, 2009. Mecp2 isoform-specific vectors with regulated expression for rett syndrome gene therapy. *PLoS One*.;4:e6810

Rossi DJ, Oshima T, Attwell D. 2000. Glutamate release in severe brain ischaemia is mainly by reversed uptake. *Nature* 403, 316–321

Sabatini BL, Regehr WG. 1997. Control of neurotransmitter release by presynaptic waveform at the granule cell to Purkinje cell synapse. *J Neurosci* 17, 3425-3435

Schipke CG, Haas B, Kettenmann H. 2008. Astrocytes discriminate and selectively respond to the activity of a subpopulation of neurons within the barrel cortex. *Cerebral Cortex*. **18**: 2450–2459.

Seki Y, Feusterl PJ, Keller RW Jr, Tranmer BI, Kimelberg HK. 1999. Inhibition of ischemia-induced glutamate release in rat striatum by dihydrokainate and an anion channel blocker. *Stroke* 30, 433–440

Skene PJ, Illingworth RS, Webb S, Kerr AR, James KD, Turner DJ, Andrews R, Bird AP. 2010. Neuronal Mecp2 is expressed at near histone-octamer levels and globally alters the chromatin state. *Mol Cell*.; 37(4):457–68.

Sofroniew MV (2009) Molecular dissection of reactive astrogliosis and glial scar formation. *Trends Neurosci* 32:638–647

Sofroniew MV, Vinters HV. Astrocytes: biology and pathology. *Acta Neuropathol* (2010) 119(1):7–35

Stipursky J, Spohr TC, Sousa VO, Gomes FCA. 2012. Neuron–astroglial interactions in cell fate commitment and maturation in the central nervous system. *Neurochem Res.* 37:2402–2418

Stout CE, Costantin JL, Naus CC, Charles AC. 2002. Intercellular calcium signaling in astrocytes via ATP release through connexin hemichannels. *J. Biol. Chem.* 277, 10482–10488

Stüttgen MC, Schwarz C. 2017. Barrel cortex: What is it good for? *Neuroscience*, 0306-4522

Takata N, Mishima T, Hisatsune C, Nagai T, Ebisui E, Mikoshiba K. 2011. Astrocyte calcium signaling transforms cholinergic modulation to cortical plasticity in vivo. *Journal of Neuroscience.* **31**:18155–65

Tang X, Kim J, Zhou L, Wengert E, Zhang L, Wu Z, Carromeu C, Muotri AR, Marchetto MC, Gage FH, Chen G. 2016. KCC2 rescues functional deficits in human neurons derived from patients with Rett syndrome. *Proceedings of the National Academy of Sciences USA.* **113**: 751-6.

Trappe, R., Laccone, F., Cobilanschi, J., Meins, M., Huppke, P., Hanefeld, F., and Engel, W. 2001. MECP2 mutations in sporadic cases of Rett syndrome are almost exclusively of paternal origin. *Am. J. Hum. Genet.* 68, 1093–1101.

Turovsky E, Karagiannis A, Abdala AP, Gourine AV. 2015. Impaired CO₂ sensitivity of astrocytes in a mouse model of Rett syndrome. *Journal of Physiology*. 593(14): 3159–68

Verkhratsky A, Orkand RK, Kettenmann H. 1998. Glial calcium: homeostasis and signaling function. *Physiological Reviews*. **78**: 99–141

Virginio C, MacKenzie A, Rassendren FA, North RA, Surprenant A. 1999. Pore dilation of neuronal P2X channels. *Nature Neuroscience* 2, 315–321

Wan, M., Lee, S.S., Zhang, X., Houwink-Manville, I., Song, H.R., Amir, R.E., Budden, S., Naidu, S., Pereira, J.L., Lo, I.F., et al. 1999. Rett syndrome and beyond: recurrent spontaneous and familial MECP2 mutations at CpG hotspots. *Am. J. Hum. Genet.* 65, 1520–1529.

Wang, X. et al. 2006. Astrocytic Ca²⁺ signaling evoked by sensory stimulation in vivo. *Nature Neuroscience*. 9, 816–823.

Williams EC, Zhong X, Mohamed A, Li R, Liu Y, Dong Q, Ananiev GE, Mok JC, Lin BR, Lu J, Chiao C, Cherney R, Li H, Zhang SC, Chang Q. 2014. Mutant astrocytes differentiated from Rett syndrome patients-specific iPSCs have adverse effects on wild-type neurons. *Human Molecular Genetics*. **23**: 2968–2980

Wu Y, Wang W, Díez-Sampedro A, Richerson GB (2007) Nonvesicular inhibitory neurotransmission via reversal of the GABA transporter GAT-1. *Neuron* 56:851–865

Yasui T, Uezono N, Nakashima H, Noguchi H, Matsuda T, Noda-Andoh T, Okano H, Nakashima K. 2017. Hypoxia Epigenetically Confers Astrocytic Differentiation Potential on Human Pluripotent Cell-Derived Neural Precursor Cells. *Stem Cell*

Reports. **8**: 1743–1756

Yang, Y. et al. 2003. Contribution of astrocytes to hippocampal long-term potentiation through release of D-serine. *Proc. Natl. Acad. Sci. USA* 100, 15194–15199.

Zhang, Q. et al. 2004. Fusion-related release of glutamate from astrocytes. *J. Biol. Chem.* 279, 12724–12733

Zonta, M. et al. 2003. Neuron-to-astrocyte signaling is central to the dynamic control of brain microcirculation. *Nat. Neurosci.* 6, 43–50